Research Square

Preprints are preliminary reports that have not undergone peer review.
They should not be considered conclusive, used to inform clinical practice,
or referenced by the media as validated information.

Deciphering EcoFitness of Marine Ecosystems through eDNA Cross-trophic Interactions

Weiye Huang
Tsinghua University
Wanqing Tai
Tsinghua University
Xiaoming Shen
Shenzhen Dapeng Peninsula Marine Library
Matteo Convertino
matteo@sz.tsinghua.edu.cn

Tsinghua University

Article

Keywords: EcoFitness, Cross-trophic Networks, Envirome, Marine Ecosystems, Allometry, Taylor's Law, eDNA

Posted Date: February 16th, 2026

DOI: https://doi.org/10.21203/rs.3.rs-8750751/v1

License: This work is licensed under a Creative Commons Attribution 4.0 International License.
Read Full License

Additional Declarations: No competing interests reported.

Deciphering EcoFitness of Marine Ecosystems through eDNA Cross-trophic Interactions

Weiye Huang[a,b], Wanqing Tai[b], Xiaoming Shen[c], Matteo Convertino[a,b,d*]

[a] Ecosystem Intelligence & Design Lab (TREES), and Nature-positive Design Hub (N^+D), Tsinghua Shenzhen International Graduate School (SIGS), Tsinghua University, Shenzhen, China

[b]Institute of Environment and Ecology, Tsinghua Shenzhen International Graduate School (SIGS), Tsinghua University, Shenzhen, China

[c]Shenzhen Dapeng Peninsula Marine Library, Shenzhen, China

[d] Shenzhen Key Laboratory of Ecological Remediation and Carbon Sequestration, Tsinghua Shenzhen International Graduate School (SIGS), Shenzhen, China

February 5, 2026

Corresponding author: * M. Convertino, Tsinghua Shenzhen International Graduate School, Institute of Environment and Ecology, Building F, office 402, lab 408, University Town of Shenzhen, Nanshan District, Shenzhen 518055, P.R. China; matteo@sz.tsinghua.edu.cn; matconv.uni@gmail.com

Keywords: EcoFitness; Cross-trophic Networks; Envirome; Marine Ecosystems; Allometry; Taylor's Law; eDNA

Abstract

Effective assessment of marine ecosystems increasingly requires approaches that go beyond static biodiversity indices to capture cross-trophic organization and dynamic stability based on network topology.

In this study, we applied a multi-marker (12S, 18S, COI) eDNA metabarcoding approach to compare the ecological organization of two subtropical ecosystems, Mirs Bay and Daya Bay nearshore and marine habitats, representing contrasting environmental settings. Species co-occurrence networks were reconstructed to examine topological features such as degree distribution, modularity, centrality, and species-pair rank, and to relate those to ecological fitness. Two ecological allometric laws were then evaluated: (1) Taylor's Power Law (TPL), which quantifies species aggregation; and (2) the Network Kleiber's Law (NKL) attributing relative species abundance (RSA) variance to network hyperconnectivity. Correlations among these ecological indicators and environmental factors were used to explore potential causal determinants of ecological organization.

The two ecosystems exhibited strikingly different network architectures. Daya Bay supported higher biodiversity and a larger, more densely connected homogeneous network, while Mirs Bay showed lower diversity and richness but a more hierarchical and compartmentalized structure. TPL described both systems well ($R^2 > 0.86$), with Mirs Bay showing stronger aggregation (ν=1.697) than Daya Bay (ν=1.460), and a more organized NKL pattern. The TPL exponent nu's sensitivity to several environmental is higher for more organized ecosystems, and increases with depth and average species biomass, suggesting its potential as a systemic ecofitness indicator of multitrophic organization. In contrast, no significant scaling relationship was found between RSA variance and network hyperconnectivity.

Significance Statement

Traditional network analyses describe structural interactions within communities, whereas ecological allometric laws summarize dynamical aggregation in species dynamics. However, these two perspectives—structural and dynamical—are rarely integrated, limiting our ability to evaluate how community organization reflects environmental adaptation and ecological fitness. The study highlights a multi-dimensional ecological fitness framework where ecological network structure and environmental dynamics jointly characterize ecosystem organization. The integration of allometric laws as morphological patterns with network topology, provides a scalable and quantitative approach for assessing ecological fitness and adaptive capacity in marine ecosystems useful for prioritized conservation and restoration under systemic environmental change and ecological dependencies.

1 Introduction

"Can One Hear the Shape of a Drum?", Mark Kac, 1966

In a seminal and elegant paper, Kac (1966) posed the question of whether a listener with perfect pitch could determine the exact shape of a drum solely by hearing its fundamental tone and overtones. This question formalizes a classic inverse engineering problem, one that is highly relevant to ecology, where the functioning of ecosystems is inferred from observed ecological patterns. A wide range of studies has engaged with this inferential challenge, for instance by looking into how space shapes time and puntuated evolution (Convertino, 2025b). However, very few studies have moved beyond morphological descriptions to examine the topology of species organization—namely, how species are assembled and interact with one another based on multimedia sensor features (such as genetical, sound, texture, etc., and their integration)—and fewer still have investigated how such topological organization can be intentionally leveraged for ecosystem engineering (including the species collective, i.e. the food web, as ecosystem engineers for nutrient, sediment and water cyclying), so as to make ecosystems "sound", that is, functioning in an optimal or desired way (i.e., bioterraformation, including the triggering of nature self-emergence from bottom-up actions, and nature eco-evolution with sensors, actuators, and infrastructure). More specifically, very few studies have investigated high-resolution, bidirectional eco–environmental flows and feedbacks structured by species' collective and vehicled by water ("eco-waves"), despite their fundamental role in habitat formation, ecosystem function (e.g., carbon cycling) and fitness (i.e., how function evolves over time). The considerations of these elements is essential in the formulation of prediction-based valuable information for ecosystem decisions (ecodesign plan, precision eco-engineering, and policy) contemplating the enhancement of ecological multifunctionality for the Earth's future. The overall idea is to charcaterize the morphology of ecological communites, via topological and functional analyses, to detect the morphology of optimal decisions triggering positive eco-environmental feedbacks.

1.1 Marine Ecosystem Criticality and eDNA

Coastal bays are among the most productive and biodiverse marine ecosystems on Earth – comprising Blue Carbon Ecosystems (Zhang and Convertino, 2024, 2025; Convertino et al., 2025) as interfacial ecosystems – providing critical habitats, nursery grounds, and ecosystem services including fisheries, water purification, and climate regulation (Halpern et al., 2008; Barbier et al., 2011; Wu and Convertino, 2025) affecting both interconnected terres-

trial and oceanic systems. However, these ecosystems face increasing pressures from climate change, pollution, and habitat degradation, highlighting the urgent need for comprehensive and timely biodiversity monitoring (Doney et al., 2012; Worm et al., 2006) that targets their ecohydrological connectivity to influence teleconnected risks and services. This is also because these ecosystems offer the highest opportunity in nature-grounded services, such as enhanced carbon sequestration, biodiversity, and water-risk reduction. Traditional survey methods, such as trawling and diving, are often invasive, costly, and heavily reliant on taxonomic expertise, limiting their effectiveness in capturing rare, cryptic, or microscopic species that affect the carbon cycle (Thomsen and Willerslev, 2015; Coleman et al., 2023).

Environmental DNA (eDNA) metabarcoding has emerged as a transformative approach for aquatic biodiversity assessment (Rishan et al., 2023; Trevathan-Tackett et al., 2019), including in the global ocean (Zhang et al., 2024b; Pierella Karlusich et al., 2025). By sequencing DNA fragments released into environmental compartments (water, soil, or air, etc), eDNA allows non-invasive, high-throughput detection of multiple species (Deiner et al., 2017; Nguyen et al., 2020). Yet, most studies have focused on single taxonomic groups (e.g., fish), overlooking the complex interactions among organisms across trophic levels (Yao et al., 2022; Djurhuus et al., 2020). To address this limitation, we employed three molecular markers-12S rRNA (fish), 18S rRNA (eukaryotes), and COI (animals, fungi, and algae)-to construct an integrated cross-trophic community framework spanning producers to consumers (Djurhuus et al., 2017; Kumar et al., 2022) in different habitats characterized by different environmental pressure. Adopting this holistic perspective allows us to probe ecosystem processes such as material cycling, energy flow, and stability (Blackman et al., 2022; McCann, 2000), and more importantly, to assess ecostem fitness.

1.2 Ecosystem Fitness as Network Topology

The common and main stake in the struggle for existence under environmental pressure is energy manifested as self-emerging networks. Energy must be divided among individuals of a species, and among different species. How this division occurs depends on self-emerging biotic interactions, both direct and indirect, shaped by feedbacks with the physical environment. These interactions may result in evolutionary changes or collapse. An evolutionary advantage in a given environmental context by one taxon instantaneously produces a net negative effect of the same magnitude across other taxa in the same adaptive zone (Liow et al., 2011), and this advantage is related to the interconnections among species. The Van Valen Red Queen Hypothesis (Liow et al., 2011; Žliobaitė, 2024) states that in comparable ecological contexts,

the probability for a taxon to survive to the next time interval is independent of how long it has already existed. However, we argue that these probabilities are largely related to the ecological community and environmental structures that are often overlooked. It is likely that, when the community's ecological network is largely random, then adaptation and evolution occur randomly, therefore species dissipate energy at much higher rate and compromise the stability and function of all interconnected ecological communities.

Maintaining stability in feedback systems, such as complex ecosystems, relies on species sensing and encoding their dynamics as a function of environmental stress (that is eco-information with decision value across trophic scales), yet by continuously adjusting their collective organization. Incremental or acute damage can make such control fragile or unstable, leading to sudden collapse or slow decay. Therefore, it is critical for species, and stakeholders, to monitor ecosystems and guranatee their rigid-flexible structure is balanced and prone to adjust ansd improve under environmental change. Ideally, positive and negative feedbacks become *neutral* the more the system reaches the critical state, that is the optimal metastable configuration in between order/rigidity and chaos/unpredictable instability. However, *criticality* can assume many forms depending on the level of organization and magnitude of eco-environmental features that define ecosystem fitness. For this reason, quantifying and mapping of ecological and environmental organization (ecograph and envirome) are necessary (Wang and Convertino, 2023b).

Building on the integrated multicommunity framework (Figure 1), cross-trophic eDNA data enable a shift from traditional species inventories toward a network-based understanding of how ecological interactions shape ecosystem structure and function (Bascompte and Jordano, 2007; Fortunato, 2010). In co-occurrence network analysis, species (or operational taxonomic units, OTUs) are represented as nodes, and their potential biotic interactions—such as mutualism, competition, or predation—are inferred from statistically significant co-occurrence patterns (Deng et al., 2012; Freilich et al., 2018). Of course these inference approaches are purely dependent on the quality of the data but they offer a powerful way to generate a topological representation of the community structure that facilitates quantitative analyses of ecosystem complexity. A growing body of evidence suggests that correlation-based co-occurrence networks, despite their inferential nature based on linearity, can effectively uncover non-random patterns of species association and potential ecological interactions due to heterogeneous abundance distributions (Barberán et al., 2012; Berry and Widder, 2014). This is particularly the case in absence of time series data for which strong causality assessment is not feasible. Moreover, the structural attributes of the inferred networks—such

as degree distribution, connectivity, modularity, and nestedness—offer powerful descriptors for assessing trophic and cross-trophic organization, ecological stability, and the system's resilience to environmental perturbations (Landi et al., 2018; Olesen et al., 2007; Zhang et al., 2024a; Thompson et al., 2012): a spatial blueprint of ecosystem dynamics over time (Convertino, 2025b). Consequently, network-based approaches have become an increasingly important framework for linking biodiversity patterns to ecosystem function and robustness under global change beyond classical macroecology (Delmas et al., 2018; Harte et al., 2022; Yan et al., 2025). The objective should be to structure species assemblage vs. counting species.

The architecture of co-occurrence networks in nearshore marine ecosystems is strongly shaped by freshwater and oceanic environmental conditions (Eskuche-Keith et al., 2023; Rogers et al., 2024), raising the question of how deeply ecological networks encode the systemic environmental pressures. Biogeochemical gradients such as temperature, salinity, and nutrient availability not only determine species dispersal and distributions through environmental filtering ("ecotaxis") but also modulate interaction strengths and configurations, thereby reshaping ecosystems' network topology and overall stability (Hou et al., 2017; Röthig et al., 2023). For instance, the combined presence of high salinity and fish predation pressure in mesotrophic waters can suppress zooplankton populations and indirectly promote algal proliferation, altering trophic link strength and community modularity (Ersoy et al., 2022; Yang et al., 2023). Beyond natural variability, anthropogenic disturbances —including nutrient enrichment, heavy metal contamination, and compounds of emerging concerns— and global climate change–induced ocean warming and acidification further intensify these environmental effects (Mok et al., 2023; Trégarot et al., 2024). Such compounded pressures can trigger pronounced shifts in community composition and interaction dynamics, making co-occurrence networks increasingly fragile and less resilient to perturbations (Convertino, 2025a). Consistent with these findings, Johnson and Angeler (2014) observed that nutrient enrichment in European streams reduced macrophyte diversity while enhancing benthic diatom diversity, reflecting a reorganization of interactions under environmental stress. Recent advances further demonstrate that eco-environmental disturbances can propagate through trophic pathways to induce systemic biogeochemical stress and early-warning shifts in chlorophyll-a dynamics, as revealed by network-based algal bloom studies (Wang and Convertino, 2023a; Wang et al., 2023). Therefore, developing a mechanistic understanding of how environmental factors regulate the structure and stability of co-occurrence networks is critical for diagnosing marine ecosystem fitness and predicting community responses in a changing ocean (Padmanabha et al., 2024; Merz et al., 2023).

1.3 Scaling Patterns, Allometric Laws, and Ecological Networks: a Unified Framework

Network-based approaches, which provide detailed structural descriptions, often lack generality across systems and scales because they do not look into how much network-defined patterns are stable and universal. Allometric laws provide a complementary framework for quantifying ecological organization, specifically by looking into how ecosystems' parts change with scales. More deeply, allometry is grounded in the search for ecological invariance and universality, that is, the stability of scaling relationships across ecological scales and geographic contexts defined by systemic environmental pressure. Typically, these allometric laws do not consider network features that define the structural and functional backbone of ecosystems, nor how these laws lead to ecosystem patterns over space. Two scaling relationships inform about the multiscale ecological organization: (i) Taylor's Power Law (TPL) captures predictable mean–variance relationships in population relative species abundance (RSA) across spatial and temporal scales (Taylor, 1961; Kilpatrick and Ives, 2003; Cohen et al., 2013; Anderson et al., 2013), and (ii) Kleiber's Law that describes how metabolic rate (related to the collective species interactions (Galbraith et al., 2022)) scales with biomass at the level of individual organisms (Kleiber, 1947; Glazier, 2014) community, or ecosystems. These patterns can be used to assess eco-fitness and to train predictive models of ecosystem change. Specifically, the Taylor's Power Law is a byproduct of species organization, while the proposed Kleiber's Law explicitly accounts for network connectivity or interaction fluxes as in Galbraith et al. (2022).

As emphasized by Marquet et al. (2005), scaling relationships are particularly valuable because they exhibit scale invariance or their breaking—retaining their form across spatial, temporal, and biological dimensions—and may reflect universal processes that structure and constrain ecological systems. In contrast to system-dependent network descriptors, and associated predictive models, scaling laws provide a parsimonious, dimensionless framework and functions capable of revealing emergent regularities that transcend particular communities or ecosystems. Their predictable patterns allow deviations from expected exponents to serve as diagnostic indicators of environmental suitability, resource-use efficiency, and system-level stability, offering a generalized means to assess how ecosystems respond to environmental stress or perturbation. Yet, deviations from optimal scaling is an assessment of ecosystem fitness as shown by Galbraith et al. (2022) and Wang and Convertino (2023b) in the context of marine ecosystems by tracing eco-environmental networks for different ecological conditions. Additionally, if the underpinning variables of allometrical laws are manageable network

factors, those factors can be used for the management and design of complex ecosystems by accounting for systemic function and fitness (Convertino, 2025b).

Recent work has begun to bridge scaling theory and ecological network: energy fluxes in food webs follow allometric regularities (Zhang and Guo, 2010), species' degree distributions in ecological networks often show power-law forms (Montoya et al., 2006; Dunne et al., 2002), and species' network centrality frequently scales with RSA (VÁZQUEZ et al., 2005; Riede et al., 2010). Complementary advances in optimal network theory likewise highlight how ecological and microbiome systems evolve toward network configurations that maximize relative stability, criticality, and information flow (Li and Convertino, 2019; Servadio and Convertino, 2018). Extending this framework, Galbraith et al. (2022) demonstrated an entropic analogue of Kleiber's Law, where total directed interactions of bacterioplankton phyla scale with community RSA organization. Building on these insights, we explore whether similar scaling regularities emerge between network topology and population variability across the inferred ecological networks under different environmental conditions. Instead of assuming a fixed relationship (such as a power-law form with a specific exponent), we tested how the form of these relationships varies across environmental contexts and network architectures. This exploratory integration aims to link structure-based and dynamics-based perspectives (i.e., topology of the network and scaling variability under environmental change) into a unified empirical framework, providing a pathway toward a predictive ecology that connects community organization and environmental pressure into ecosystem fitness (Winemiller et al., 2001; Pietro et al., 2018; Deyle et al., 2016; Zhang and Convertino, 2024, 2025). This information is highly useful to prioritize conservation and restoration efforts that enhance the function of ecosystems as a whole including eco-environmental flows.

1.4 Pearl River Delta Marine Ecosystems as Archetypes for Eco-Fitness

This study leverages the ecological data gathered from two weakly dependent and environmentally distinct subtropical marine ecosystems in the Pearl River Delta, South China Sea: Mirs Bay and Daya Bay sites. By implementing a comprehensive multi-marker eDNA strategy (12S rRNA for fish, 18S rRNA for eukaryotes, and COI for animals, fungi, and algae), we reconstructed cross-trophic co-occurrence networks, spanning producers to consumers, enabling a comparative analysis of community structure, network topology (including degree distribution, modularity, and connectivity), and the underlying environmental drivers. Cru-

cially, we integrated network analysis with aloometric laws—specifically, Taylor's Power Law (TPL) describing mean–variance relationships and a novelly introduced "Network Kleiber's Law" (NKL) linking hyperconnectivity (as the total number of interdependent species) to the variance of species—to establish a quantitative framework for diagnosing deviations from expected laws and ecological organization that signal environmental stress or adaptive responses. The overarching goal is to establish an "eco-informatic" framework for assessing ecological fitness by deciphering the eDNA-based core structural and functional differences between these nearshore marine ecosystems, thereby advancing our fundamental understanding of marine ecohealth, stability, and resilience under global and local anthropogenic change (Winemiller et al., 2001; Pietro et al., 2018; Deyle et al., 2016). Ultimately, this work is designed not only to provide new perspectives for biodiversity assessment but also to deliver a scalable scientific framework for predicting multiscale population features that can guide regional monitoring, global marine resource management, and strategic responses to climate and local change informed by high-resolution ecological information.

2 Materials and Methods

2.1 Eco-Environmental Data Collection

This study is based on samples collected from two marine ecosystems in the eastern waters of Hong Kong, both belonging to the South China Sea: Mirs Bay and Daya Bay (Fig. 2); the former a coastal site, and the latter is a marine island site. Sampling was conducted in Mirs Bay in September 2023 across four microhabitats—Shallow Reef (SR), Coral Nursery (CN), Deep Rocky (DR), and Rocky Reef (RR) (Fig. 2C)—with water samples collected at three depths (surface, middle, bottom). See Figure 2 for locations, and the Glossary for specifics about the sampled sites. In Daya Bay, surveys took place in September 2022 at four stations (HO1, HO2, XI, and IL) (Fig. 2C), with samples taken at two depths (surface and middle). All samples were preserved in sterile bottles, transported on ice to the laboratory within 4 h, and immediately filtered through 0.45 μm mixed cellulose ester (MCE) membrane filters (Li et al., 2018). Filters were then sealed in sterile tubes and stored at –20 °C until DNA extraction (Spens et al., 2016).

Environmental data (Table S1) (temperature, dissolved oxygen, nitrogen oxides, chlorophyll-a, and salinity as shown in Fig. 2D) were obtained from WavyOcean (The Hong Kong University of Science and Technology, 2025), a GIS-based dynamic visualization system for

multi-source, heterogeneous marine data. Corresponding environmental values for each sample were extracted based on its geographic coordinates and sampling depth. Environmental values are year averages considering predicted daily data from 1992. This platform visualizes observational data from marine stations alongside multi-scale simulations and forecasts of the marine-atmospheric-biogeochemical environment for the Guangdong-Hong Kong-Macao Greater Bay Area, enabling three-dimensional reconstruction, real-time rendering, and dynamic display of massive datasets.

2.2 DNA Extraction, Sequencing, and Processing

Genomic DNA was extracted from all samples by Magigene, Shenzhen and Guangzhou, China (https://www.magigene.com/) using commercial kits according to the manufacturer's protocols (Deiner et al., 2017; Hinlo et al., 2017), and the DNA concentration was quantified using a Qubit fluorometer. For PCR amplification (Leray and Knowlton, 2015), barcoded primers were designed to target specific regions of the mitochondrial 12S, 18S, and COI genes (see Table S2 for details). The resulting amplicons were sequenced on an Illumina NovaSeq 6000 platform by Magigene (Shenzhen and Guangzhou, China) (Ruppert et al., 2019).

The raw sequencing data (Raw Reads) were first subjected to rigorous quality control. Magigene used Fastp software to perform quality control on the raw sequences, removing adapter sequences, low-quality bases, and sequences of insufficient length, resulting in high-quality clean data (Clean Reads). Then, the filtered paired-end reads were assembled using the USEARCH software (v11.0.667) (default selection of 350,000 reads, or all reads if fewer than 350,000 were available) (Edgar, 2010). The VSEARCH software was used to remove primer sequences based on the alignment results at both ends of the primers, as well as sequences with sequencing errors exceeding 1% (Rognes et al., 2016). All assembled sequences from all samples were merged, and duplicate sequences were removed using VSEARCH software, retaining only representative sequences with RSA greater than 4. Subsequently, sequences were clustered based on similarity levels to generate operational taxonomic units (OTUs) and their RSA tables. OTUs were classified and annotated at the species level using BLAST (v2.2.31) against the Magigene company's proprietary database.

2.3 Species Composition and Biodiversity Analysis

After obtaining species annotation information for each OTU, we performed statistical analysis of species composition at the family taxonomic level. By calculating the RSA of each family across different samples, we analyzed and compared the dominant groups revealed

by the two bays under different molecular markers. To quantify and compare species diversity across samples, we used the vegan package to calculate alpha diversity indices based on OTUs, including species richness and Shannon diversity index (Oksanen et al., 2022).

2.4 Co-occurrence Network Construction and Characterization

2.4.1 Network Inference

To explore the interaction patterns among species in the ecosystems of the two bays, we constructed co-occurrence networks for Mirs Bay and Daya Bay, respectively. The networks were constructed based on the RSA data of all OTUs integrated from the 12S, 18S, and COI markers. To reduce the interference of rare species on correlation calculations, we first filtered the data, retaining only OTUs present in more than 25% of the samples for subsequent analysis.

Co-occurrence networks across trophic levels were constructed based on Spearman's correlation. A significant co-occurrence relationship between two OTUs was defined when the absolute value of the correlation coefficient exceeded 0.75 and the associated P-value was less than 0.05, following Friedman et al. (2012). Each node in the network represents an OTU, and edges denote significant pairwise associations. The networks were visualized using the igraph library (v2.1.4) (Csárdi and Nepusz, 2006). Node classification was determined according to OTU taxonomic annotation, including algae, arthropods, fungi, fish, mollusks, protists (non-algal), other animals, and unclassified groups. To further illustrate the composition of inter-group interactions, pie charts were generated to display the proportional distribution of links among different node categories.

2.4.2 Network Topological Analysis

To further characterize the structural features of the constructed co-occurrence networks, we calculated a series of topological metrics, that systemic features and their distributions, using the `igraph` package (v2.1.4) in R (Csárdi and Nepusz, 2006). These metrics are divided into **node-level** and **network-level** properties (i.e., OTUs and communities), providing a comprehensive view of both local connectivity and global network organization.

Node-level metrics. Node-level metrics describe the local connectivity and structural importance of individual node within the network.

- **Degree (k_i)** — the number of direct connections of node i:

$$k_i = \sum_{j=1}^{N} a_{ij} \tag{2.1}$$

  where $a_{ij} = 1$ if nodes i and j are connected, otherwise $a_{ij} = 0$.

- **Shortest path length (L_i)** — the average shortest distance from node i to all other nodes:

$$L_i = \frac{1}{N-1} \sum_{j \neq i} d_{ij} \tag{2.2}$$

- **Clustering coefficient (C_i)** — quantifies the tendency of node i's neighbors to be mutually connected, forming closed triangles:

$$C_i = \frac{2t_i}{k_i(k_i - 1)} \tag{2.3}$$

  where t_i is the number of triangles including node i, and k_i is the degree of node i.

- **Betweenness centrality (B_i)** — quantifies the fraction of shortest paths passing through node i:

$$B_i = \sum_{s \neq i \neq t} \frac{\sigma_{st}(i)}{\sigma_{st}} \tag{2.4}$$

  where σ_{st} is the total number of shortest paths between nodes s and t, and $\sigma_{st}(i)$ is the number of paths passing through node i.

Network-level metrics. Network-level metrics capture global structural features of the co-occurrence network. They include direct network properties as well as network-wide summaries of node-level metrics.

- **Number of nodes (N)** — total number of OTUs in the network.

- **Network density (D)** — the ratio of observed edges (E) to the maximum possible number of edges in an undirected network:

$$D = \frac{2E}{N(N-1)} \tag{2.5}$$

- **Network diameter ($L_{\max}$)** — the longest shortest path between any two nodes:

$$L_{\max} = \max_{i,j} d_{ij} \tag{2.6}$$

- **Average node-level metrics** — network-wide summaries of node-level properties, including: Average degree, shortest path length, clustering coefficient, and betweenness centrality:

$$\langle k \rangle = \frac{1}{N}\sum_{i=1}^{N} k_i, \quad \langle L \rangle = \frac{1}{N}\sum_{i=1}^{N} L_i, \quad \langle C \rangle = \frac{1}{N}\sum_{i=1}^{N} C_i, \quad \langle B \rangle = \frac{1}{N}\sum_{i=1}^{N} B_i \tag{2.7}$$

2.5 Taylor's Power Law (TPL)

To quantify species aggregation patterns within the marine ecosystems, Taylor's Power Law (TPL) was applied to OTU RSA data. The mathematical expression for this law is (Taylor, 1961):

$$\sigma^2(\text{RSA}) \sim c \cdot \mu(\text{RSA})^{\nu} \tag{2.8}$$

where c and ν are fitted constants. The exponent ν serves as an index of aggregation: $\nu > 1$ indicates aggregated (clumped) distribution, $\nu \approx 1$ indicates random distribution, and $\nu < 1$ indicates uniform or regular distribution (Cobain et al., 2018b).

2.6 Network-theoretic Kleiber's Law (NKL)

To explore how the functional role of species within ecological networks relates to their stability in terms of RSA variance (instead of entropy based on distributions that are hard to infer without long time series), we proposed a Network-theoretic Kleiber's Law (NKL). This approach extends the classical scaling theory to network topology, using co-occurrence networks constructed from Mirs Bay and Daya Bay microbial communities.

Relative Species Abundance Fluctuations. This metric quantifies the variability of each OTU's RSA with respect to the mean, represented by its variance across sampling sites. A higher variance reflects greater stability or fluctuations in RSA that are highly correlated with each other according to different distribution in between order and chaos.

$$\sigma_i^2 = \frac{1}{N-1}\sum_{t=1}^{N}(RSA_{i,k} - \langle RSA \rangle_i)^2 \tag{2.9}$$

where:

- σ_i^2 is the RSA variance of OTU i;
- $RSA_{i,k}$ is the RSA of OTU i at sampling site k;

- $\langle RSA \rangle_i$ is the mean RSA of OTU i across all sampling sites;
- N is the total number of samples (communities at different depths).

Hyperconnectivity. The hyperconnectivity (H_i) of each OTU characterizes its total interaction capacity within the network, integrating, implicitly, both direct and indirect connections. Here, hyperconnectivity is expressed as the cumulative connectivity of a node/species, quantified through the sum of shortest path lengths, forming tree-like networks, to all other nodes, as:

$$H_i = \sum_{j \neq i} d_{i,j} \ , \tag{2.10}$$

where:

- H_i denotes the hyperconnectivity (sum of all shortest paths, i.e. trees, from i to j) of OTU i;
- $d_{i,j}$ represents the shortest path length (number of steps) between OTUs i and j.

Hypothetical NKL Scaling. To examine the intrinsic coupling between RSA fluctuations and hyperconnectivity, we hypothesized a power-law scaling analogous to Kleiber's law:

$$H \sim (\sigma^2)^{\epsilon} \tag{2.11}$$

where H represents the hyperconnectivity of the species in the inferred co-occurance network, σ^2 denotes the variance of RSA, and ϵ is the hypothetical scaling exponent describing how RSA fluctuations scale with hyperconnectivity. This hypothesis was tested against the data assuming the correlation-based inference of species networks.

2.7 Statistical Analyses

Spearman correlation analysis was used to assess the strength and significance of correlations among environmental factors (Chen et al., 2019). For sampling sites in Mirs Bay and Daya Bay, Spearman correlation coefficients (r) were calculated between each environmental factor (temperature, dissolved oxygen, chlorophyll-a, salinity, and nitrate), and significance levels were determined using two-tailed tests (p ¡ 0.05 indicates significant, p ¡ 0.01 indicates extremely significant).

Mantel tests were used to assess the correlation between community composition and environmental factors . By constructing an environmental distance matrix (based on standardized environmental factor data using Euclidean distance) and a biological distance matrix (based

on community composition data using Bray-Curtis distance), the Mantel test was used to calculate the correlation (Mantel's r) and significance (p-value) between the two matrices.

To investigate local network structure at individual sampling sites, sub-networks were extracted using the `subgraph()` function in the `igraph` package (Csárdi and Nepusz, 2006), retaining only nodes and edges corresponding to OTUs detected at the focal site. This allowed site-specific network topology to be analyzed independently. Univariate linear regression models were fitted to evaluate the relationships between environmental factors and network topology metrics. Each topological parameter (e.g., degree, clustering coefficient, average shortest path length, betweenness centrality) was treated as a response variable, and each environmental factor was treated as a predictor. Models were fitted using the `lm()` function in R, with goodness-of-fit assessed by the coefficient of determination (R^2) and significance determined via p-values.

3 Results

3.1 Community Composition and Diversity Structure

3.1.1 Species Composition Across Multiple Taxonomic Groups

Analyses based on the 12S, 18S, and COI markers consistently distinguished the species of Mirs Bay and Daya Bay, while each marker captured complementary dimensions of biodiversity.

For the 12S rRNA gene, the two bays harbored distinct fish faunas (Fig. 3A). In Mirs Bay, fish communities showed high intra-bay heterogeneity, with dominant families (*Gerreidae*, *Clupeidae*, *Siganidae*, and *Mugilidae*) varying across sites and depths. In contrast, fish communities in Daya Bay were relatively uniform, with *Clupeidae*, *Siganidae*, and *Cyprinidae* consistently dominant across most samples.

The 18S rRNA gene analysis indicated the opposite pattern in eukaryotic communities (Fig. 3B). In Mirs Bay, nearly all samples were dominated by *Rhizosoleniaceae* (¿50% RSA), resulting in low within-bay variability. In Daya Bay, however, the eukaryotic community was more evenly distributed among several dominant families, including *Thalassiosiraceae*, *Stephanodiscaceae*, and *Cymatosiraceae*.

The COI gene analysis, targeting animals, fungi, and algae, reinforced the distinction between the two bays (Fig. 3C). Communities in Mirs Bay displayed high internal variability, with

dominant groups such as *Rhizosoleniaceae* (algae), *Bacillariaceae* (algae), *Gymnodiniaceae* (algae), and *Ostreidae* (animals) alternating among samples. By contrast, almost all Daya Bay samples were consistently dominated by *Skeletonemataceae* (algae) and *Mamiellaceae* (algae) (together ¿50%).

Overall, all three genetic markers revealed clear compositional differences between Mirs Bay and Daya Bay. The species richness distribution dependent on the Relative Species Abundance (Preston's plot), shown in Fig. S1 and S2, shows patterns in between the Fisher's logseries and the lognormal distribution. The tail of these distribution is longer for Mirs Bay than Daya bay; yet, the maximum abundance is one order of magnitude larger for Mirs Bay despite richess is larger for the latter. This confirms the hypothesis that species organization, also manifested by the more lognormal Preston's plot, is a sign of ecofitness rather species count.

3.1.2 Contrasting Diversity Patterns Between and Within Bays

Alpha diversity analysis (Fig. 4) revealed two consistent patterns: (1) overall biodiversity was significantly higher in Daya Bay than in Mirs Bay across all metrics, and (2) the spatial organization of diversity differed markedly within each bay.

The strongest disparity occurred in species richness. For the fish community (12S), Daya Bay harbored substantially more OTUs (44–118) than Mirs Bay (2–49). This contrast was even greater for 18S and COI markers, where richness in Daya Bay (2091–2800 and 3993–5339 OTUs, respectively) was several-fold higher than in Mirs Bay (451–606 and 747–1026 OTUs). Shannon indices mirrored these trends: values derived from 18S and COI were consistently higher in Daya Bay, indicating both greater richness and more even communities, whereas 12S-based Shannon values were closer between bays but remained higher in Daya Bay.

Within-bay patterns further emphasized these contrasts. In Mirs Bay, 18S-derived Shannon indices varied little among sites, consistent with the dominance of *Rhizosoleniaceae* (Fig. 3B). In contrast, 12S and COI datasets exhibited pronounced spatial heterogeneity, with large differences among sites (CN, DR, RR, SR). In Daya Bay, the opposite pattern was observed: 12S and COI communities were relatively uniform across sites (HO1, HO2, IL, XI), while 18S displayed marked heterogeneity, with HO1 and HO2 showing notably higher Shannon values ($\sim$5.6) than IL and XI ($\sim$4.15).

Taken together, these observations highlight the contrasting diversity structures of the two bays. Daya Bay exhibits higher overall biodiversity, characterized by relatively homogeneous

fish and metazoan–algal–fungal communities but greater heterogeneity among eukaryotic assemblages, whereas Mirs Bay shows lower total diversity, yet stronger spatial variability across markers.

3.2 Co-occurrence Network Structure and Topological Analysis

3.2.1 Network Architecture and Interaction Distribution

Cross-trophic co-occurrence networks (Fig. 5A) revealed clear contrasts between the two bays in scale, complexity, and interaction patterns. The Daya Bay network (5,862 nodes, 9,634 edges) was substantially larger than that of Mirs Bay (842 nodes, 1,154 edges). Node categories in both networks included algae, arthropods, fungi, fish, mollusks, non-algal protists, other animals, and unclassified groups.

Despite similar node categories, the distribution of edge types (Fig. 5B) differed markedly. In Mirs Bay, interactions were dominated by algae, with algae–algae (27.8%), algae–unclassified (25.6%), and algae–protist (7.7%) edges comprising the majority of links. In contrast, Daya Bay displayed a more balanced edge distribution. The most frequent interactions involved unclassified groups (unclassified–unclassified, 23.8%; algae–unclassified, 15.1%; arthropod–unclassified, 13.2%), followed by algae–protist (9.4%) and algae–algae (9.1%).

3.2.2 Network Topological Features

Distributions of node-level key topological parameters (Fig. 5C) revealed clear contrasts between the Daya Bay and Mirs Bay networks.

Degree values were distributed across a wider range in Daya Bay compared to Mirs Bay. In Mirs Bay, degrees were strongly right-skewed, concentrated at low values below 200, while Daya Bay exhibited an extended right tail, with degrees exceeding 1,500 and several prominent peaks between 400 and 600.

Average Path Length (APL) distributions showed a clear distinction between the two sites. Mirs Bay displayed a bimodal pattern, with one sharp peak at approximately 1.0 and a broader distribution centered near 2.7. Daya Bay, by contrast, exhibited a narrower, multimodal distribution between 1.7 and 2.3, with the majority of nodes around 1.9.

Betweenness Centrality (BC) values were right-skewed in both bays. In Mirs Bay, most nodes had BC values near zero, while a small number exhibited high BC values above 1×10^5. Daya Bay also showed a concentration near zero but with a broader spread, extending into the low-to-medium BC range (up to 5×10^4).

Clustering Coefficient (CC) distributions differed markedly between the two bays. In Mirs Bay, the CC distribution was strongly bimodal, with most nodes exhibiting low to moderate values (0.0–0.5, peak around 0.35) and a sharp secondary peak at 1.0. In contrast, Daya Bay showed a narrower, unimodal distribution concentrated between 0.25 and 0.50 (centered at 0.35–0.40), with a minor secondary peak near 0.90.

3.3 Ecological Patterns: Aggregation and Network Organization

3.3.1 Species Aggregation: Taylor's Power Law

Using Taylor's Power Law (TPL) as an analytical framework, we examined RSA variability patterns in Mirs Bay and Daya Bay. Both datasets closely followed the power-law relationship defined by TPL (Fig. 6 A and B). On loglog scales, the mean and variance of RSA exhibited a significant power-law relationship, with coefficients of determination (R^2) of 0.916 for Mirs Bay and 0.861 for Daya Bay, and systemic aggregation exponents (ν) of 1.697 and 1.460, respectively, indicating strong community-level aggregation.

Taxon-specific TPL analyses (Fig. S5 and S6) of eight major groups confirmed pervasive aggregation across taxa, with all groups showing ν values greater than 1. In most groups, Mirs Bay exhibited higher aggregation than Daya Bay, with ν values ranging from 1.58 to 1.85, compared with 1.31 to 1.74 in Daya Bay; specifically, algae (1.67 vs. 1.48), arthropods (1.62 vs. 1.55), fungi (1.65 vs. 1.44), mollusks (1.79 vs. 1.74), other animals (1.85 vs. 1.72), non-algal protists (1.63 vs. 1.49), and unclassified taxa (1.58 vs. 1.31). Fish assemblages were an exception, showing the highest aggregation in both bays, with ν values approaching 2.0; Fish in Daya Bay had a slightly higher ν (2.05) than in Mirs Bay (1.95).

3.3.2 RSA Variability and Hyperconnectivity: Network Kleiber's Law

To quantify the relationship between RSA variability and network structure, we plotted the variance of each OTU's RSA against its hyperconnectivity (the sum of shortest-path lengths to all other nodes, i.e. a branching tree maximizing information dependency among interconnected components) on log–log axes for Mirs Bay and Daya Bay (Fig. 6 C and D).

Across both ecosystems, no significant scaling relationship was observed between RSA variance and hyperconnectivity. The data points formed scattered clusters with an overall near-zero slope on log–log axes, indicating that RSA variability was independent of network position.

Further validation (Fig. S7 and S8) was obtained through separate analyses of eight major

taxonomic groups (algae, arthropods, fish, fungi, mollusks, non-algal protists, other animals, and unclassified OTUs). Across all groups, the relationship between RSA fluctuations and hyperconnectivity was consistent with the overall pattern, showing no detectable scaling relationship in either species.

3.4 Envirome-Biocomplexity Nexus

3.4.1 Contrasting Environmental Regimes on Communities: Ecograph-Envirome Coupling

Analyses of community–environment relationships revealed fundamentally different degrees of environmental coupling in the two bays (Fig. 7 A and B). Mirs Bay displayed tightly coupled environmental variables, whereas Daya Bay exhibited more loosely associated environmental variables.

In Mirs Bay, the upper correlation matrix shows a dense web of associations, with temperature serving as a central hub—positively correlated with salinity and chlorophyll-a, and negatively with oxygen (Spearman's r, all $p < 0.001$). In contrast, the Daya Bay matrix was much sparser. A striking difference was the role of chlorophyll-a: highly interconnected in Mirs Bay, but statistically isolated in Daya Bay, showing no significant correlations with other measured variables.

These divergent regimes were reflected in community–environment linkages revealed by Mantel tests (Fig. 7 A and B). In Mirs Bay, multiple environmental variables broadly influenced community structure, with chlorophyll-a emerging as the predominant driver, exhibiting strong correlations with most biological groups (Mantel's $r > 0.7$, $p < 0.01$). By contrast, Daya Bay communities were shaped primarily by salinity and chlorophyll-a, both of which showed robust associations with several key taxa.

3.4.2 Environmental Imprinting on Ecological Network Structure

talk about the magnitude of env factors beyond their organization To assess environmental responses, sub-networks were extracted from each sample, and their topological parameters were calculated (Figs. S3, S4, S9 and S10). At this fine-grained scale, network sizes were consistently larger in Daya Bay than in Mirs Bay. Node counts per station in Mirs Bay ranged from 608 to 725 (edges: 761–995), whereas in Daya Bay they ranged from 3,540 to 4,704 (edges: 4,373–7,400), reflecting higher potential interaction complexity in Daya Bay. However, just the sheer number of edges does not reveal the organization of complexity, and yet the ecological fitness of an ecosystem.

Sub-networks within each bay exhibited distinct topological patterns. Mirs Bay sites (SR, CN, DR, RR) displayed centralized structures, with a core of hub nodes (primarily algae) surrounded by peripheral nodes. In contrast, Daya Bay sites (HO1, HO2, XI, IL) showed more diffuse structures, lacking a single dominant hub and exhibiting widespread connections among nodes. Networks for all communities highlight the same network topology at the ecosystem scale (Figs. S3 and S4).

Linear regression analysis indicated a contrasting response of network topology to environmental factors. In Mirs Bay, several topological parameters were significantly correlated with multiple variables ($P < 0.05$). For example, the clustering coefficient was negatively correlated with chlorophyll-a and salinity ($R = -0.83$), and positively correlated with dissolved oxygen and temperature ($R = 0.83$). Network diameter showed correlations of similar magnitude (absolute $R \approx 0.65$) but in the opposite direction to the clustering coefficient.

In Daya Bay, most topological parameters were not significantly correlated with environmental factors ($P > 0.05$). Where correlations existed, their magnitude was generally higher than in Mirs Bay (Figs. S9 and S10). For instance, network diameter showed a strong positive correlation with salinity ($R = 0.91$) and strong negative correlations with dissolved oxygen and temperature ($R = -0.81$ vs. $R \approx -0.65$ in Mirs Bay). This indicates that while fewer factors shape the Daya Bay network, its structure is exceptionally sensitive to shifts in key physical drivers.

3.4.3 Environmental Drivers of Taylor's Power Law

To evaluate the influence of environmental factors on community structure, we analyzed the linear relationships between the Taylor's Power Law (TPL) exponent and five key environmental variables (Fig. 7C): chlorophyll-a, nitrate, dissolved oxygen, salinity, and temperature.

The TPL exponent exhibited strong and statistically significant response to multiple environmental factors (Fig. 7C). Specifically, TPL was highly positively correlated with temperature ($R^2 = 0.85$, $P < 0.001$) and significantly positively correlated with dissolved oxygen ($R^2 = 0.45$, $P = 0.001$), while it showed a significant negative correlation with chlorophyll-a concentration ($R^2 = 0.51$, $P < 0.001$). In contrast, no significant linear relationships were detected between the TPL exponent and either nitrate or salinity.

A pronounced regional differentiation was also observed: across all environmental gradients, samples from Mirs Bay consistently exhibited higher TPL exponents and stronger aggregation

than those from Daya Bay. The median TPL exponent in Mirs Bay (~ 1.81) was significantly higher than in Daya Bay (~ 1.65), with non-overlapping distributions, confirming systematic inter-regional differences in aggregation patterns.

3.4.4 Ecological Integration: Coupling of TPL Aggregation and Network Topology

We further examined the relationships between the TPL exponent and key network topological parameters (Fig. S10). Networks characterized by higher community aggregation (higher TPL exponent) tend to have smaller size (node number, strongly negatively correlated, $R^2 = 0.97$), higher overall connectivity (network density, strongly positively correlated, $R^2 = 0.96$), greater structural centrality (betweenness centrality, strongly positively correlated, $R^2 = 0.90$), and lower modularity (clustering coefficient, strongly negatively correlated, $R^2 = 0.94$).

Across all metrics, samples from Mirs Bay and Daya Bay formed distinct clusters, with Mirs Bay consistently exhibiting higher TPL values, indicating tighter internal coupling between aggregation intensity and network structure.

4 Discussion

4.1 eDNA: A New Perspective for a Systemic Biocomplexity Fitness

Mirs Bay and Daya Bay, as important and interconnected ecosystems in the South China Sea, harbor rich biodiversity that carries valuable ecological and biogeographical information. This biodiversity reflects regional environmental gradients and adaptive processes, providing a crucial baseline for marine research and conservation. However, systematic biodiversity surveys, especially those targeting entire multi-trophic communities, have long been challenged by the region's complex hydrodynamics and intense anthropogenic disturbances (Diao et al., 2022). Consequently, previous studies in these bays have often been limited to specific biological groups, such as fish or plankton, failing to provide a holistic view of the ecosystems (Wu et al., 2023).

Our research addresses this gap by systematically mapping the biodiversity patterns of both bays using multi-marker eDNA analysis. The results confirm that these bays not only harbor abundant aquatic life but also that communities in different water layers and sub-regions contribute unique and irreplaceable components to the overall biodiversity. Specifically, analyses across the 12S, 18S, and COI markers consistently distinguished the species compositions of

Mirs Bay and Daya Bay, with each marker capturing complementary dimensions of biodiversity: 12S highlighting distinct fish faunas, 18S revealing eukaryotic community patterns, and COI reinforcing differences in metazoan-algal-fungal assemblages. Alpha diversity metrics further underscored these contrasts, showing significantly higher overall biodiversity in Daya Bay across all markers, coupled with bay-specific spatial heterogeneity—such as uniform fish and COI communities in Daya Bay versus high variability in Mirs Bay.

However, it is essential to acknowledge the sources of uncertainty inherent in eDNA metabarcoding for whole communities, as highlighted in recent analyses (Jones et al., 2025). These uncertainties arise across multiple stages: (1) sampling variability, including spatial and temporal heterogeneity in eDNA shedding, transport, and degradation influenced by environmental factors like water flow and temperature; (2) technical biases during laboratory procedures, such as DNA extraction efficiency, PCR amplification preferences for certain taxa, and sequencing errors due to depth or platform variations; (3) bioinformatics challenges, encompassing OTU clustering thresholds, chimera removal, and inaccuracies in taxonomic assignment stemming from incomplete reference databases; and (4) interpretive limitations, where false positives/negatives or quantification issues can affect community metrics and biomonitoring reliability. Despite these challenges, careful experimental design, replication, and integration with traditional methods can mitigate uncertainties, ensuring robust inferences for ecosystem assessment.

Therefore, our work confirms that eDNA-based analysis is not only an effective approach for comprehensively characterizing bay ecosystems but also provides a powerful new tool for biodiversity assessment and conservation across broader ecological scales — by simultaneously capturing multiple trophic level organization, revealing spatial biodiversity gradients between and within bays. These findings lay the groundwork for exploring ecological processes through species co-occurrence and interaction patterns, as detailed in the following section.

4.2 Advantages and Ecological Implications of Multi-trophic Co-occurrence Networks

Building upon the biodiversity patterns revealed by multi-marker eDNA analysis, we further examined the underlying ecological interactions by constructing multi-trophic co-occurrence networks integrating 12S, 18S, and COI data. This network-based framework extends traditional diversity assessments by linking taxonomic composition to the structural and functional organization of marine ecosystems.

Consistent with the diversity contrasts between the two bays, the networks exhibited pronounced differences in scale and topology. The Daya Bay network contained over seven times more nodes and nine times more edges than that of Mirs Bay, reflecting both higher biodiversity and greater interaction complexity (in terms of magnitude and not organization that is reflected by the distribution of network features). While node categories were broadly similar—comprising algae, arthropods, fungi, fish, mollusks, protists, and unclassified groups—the interaction composition diverged substantially. Mirs Bay was dominated by algae-centered links (e.g., algae–algae and algae–unclassified), suggesting a relatively simplified, phytoplankton-driven structure. In contrast, Daya Bay displayed a more balanced interaction profile, with frequent associations among unclassified taxa, arthropods, and algae, indicative of denser cross-trophic linkages and enhanced functional connectivity.

Despite its smaller scale, the Mirs Bay network exhibited a more pronounced scale-free topology. Its degree distribution followed a steep right-skewed pattern dominated by numerous low-degree nodes and a few highly connected hubs. This structure is characteristic of self-organized, scale-free systems that are robust to random species loss but vulnerable to targeted removal of key nodes. The scale-free topology is likely shaped by the more log-normal Preston plot of RSA as show in Figure S1. Daya Bay, by contrast, displayed a broader, multimodal degree distribution with a more even spread of medium- to high-degree taxa. Such a pattern suggests greater overall connectivity but a departure from strict scale-free organization, potentially increasing vulnerability to cascading effects once perturbations occur in densely linked regions.

Average Path Length (APL) and Betweenness Centrality (BC) patterns supported these contrasting organizational modes. The bimodal APL distribution in Mirs Bay indicates a compartmentalized network where communication is efficient within clusters but limited across modules—an architecture consistent with localized stability under variable conditions. Daya Bay exhibited shorter and narrower APL values, suggesting more cohesive but less modular connectivity. Meanwhile, Mirs Bay's BC distribution was dominated by a few critical intermediaries, reinforcing the idea of hierarchical control typical of scale-free systems, whereas Daya Bay displayed more evenly distributed BC values, implying greater redundancy in cross-module interactions.

Clustering Coefficient (CC) distributions further differentiated the two systems. Mirs Bay displayed a pronounced bimodal "U-shaped" pattern, combining both loosely connected taxa and highly clustered local modules. Daya Bay, in contrast, exhibited a single dominant peak at moderate CC values (0.35–0.40), reflecting a more homogeneous modular structure.

These differences suggest that Mirs Bay supports a compartmentalized but resilient topology shaped by selective environmental pressures, while Daya Bay represents a dense, interaction-rich system that may facilitate energy transfer but randomly, yet at the cost of higher energy dissipation and structural fragility under stress (that is the antithesis of resilience).

Overall, these findings highlight that higher biodiversity and connectivity do not necessarily translate into greater network resilience. Mirs Bay's scale-free, hierarchically organized network appears optimized for persistence under resource limitation, whereas Daya Bay's highly connected but less modular structure supports high productivity and interaction turnover. By integrating cross-marker molecular data and network topology, multi-trophic co-occurrence analysis provides a powerful framework to interpret how diversity patterns translate into structural resilience, functional redundancy, and ecological stability in marine ecosystems. The average value of network metrics for both bays are show in Table S3.

4.3 Species Aggregation Revealed by Taylor's Power Law

Our application of Taylor's Power Law (TPL) revealed distinct aggregation patterns between Mirs Bay and Daya Bay, with both bays conforming to the expected power-law relationship between mean RSA and variance (high R^2 values of 0.916 and 0.861, respectively). The higher overall TPL exponent in Mirs Bay ($\nu = 1.697$) compared to Daya Bay ($\nu = 1.460$) indicates stronger community-level aggregation in the former, a pattern largely consistent across taxonomic groups, where Mirs Bay exhibited elevated ν values in most categories (e.g., Algae: 1.67 vs. 1.48), except for fish, which showed high aggregation in both bays approaching 2.0. Furthermore, Mirs Bay displayed a narrower range of ν values, suggesting more defined aggregation strategies across trophic levels, while Daya Bay's wider spectrum reflects greater variability among groups.

These findings underscore TPL's feasibility as an indicator of ecological fitness, as the exponent ν quantifies species aggregation (or portfolio effects as in Anderson et al. (2013)) in response to environmental conditions (Cobain et al., 2018a). Mechanistically, TPL captures how environmental variability influences community structure. While lower ν values can indicate more uniform distributions, the higher ν value in Mirs Bay suggests that intensified aggregation may be a key adaptive strategy. This stronger aggregation, coupled with Mirs Bay's tighter environmental coupling, implies a highly structured and specialized community co-evolved with its environment, potentially reflecting higher ecological fitness compared to the looser associations in Daya Bay. In our study, the strong positive correlations of TPL exponents with temperature ($R^2 = 0.85$) and dissolved oxygen ($R^2 = 0.45$), alongside a neg-

ative correlation with chlorophyll-a ($R^2 = 0.51$), demonstrate how physicochemical gradients precisely modulate this adaptive aggregation.

Integrating TPL with network topology further elucidates these mechanisms: higher exponents correlated with increased density ($R^2 = 0.96$), greater centrality ($R^2 = 0.90$), and reduced modularity ($R^2 = 0.94$), patterns that clustered distinctly by bay. This strongly suggests that the stronger aggregation (high ν) in Mirs Bay fosters a more efficient, centralized, and densely connected network, even though its overall size is smaller. This low-modularity, high-centrality structure is not a sign of instability, but rather indicates a highly optimized and robust configuration for resource and information flow, reinforcing TPL's role in assessing this specialized form of high fitness.

Overall, by linking aggregation to environmental drivers and network structure, TPL offers a robust, scale-invariant metric for diagnosing ecosystem fitness, with potential applications in monitoring marine responses to global and local anthropogenic change.

4.4 RSA Variability and Node Hyperconnectivity Pattern

The analysis revealed no significant scaling relationship between RSA variability and node hyperconnectivity (Fig. 6 C and D), indicating a decoupling between species dynamics and network structure in both bays. While prior studies have suggested that species with high RSA variability may serve as hubs influencing network stability and function, our results diverge—showing near-zero slopes on log–log axes, where highly connected nodes exhibit neither enhanced nor reduced variability compared to peripheral ones.

This independence also suggests that network centrality does not directly determine species stability. Instead, ecological resilience may emerge from structural redundancy and compensatory dynamics, where perturbations at one node are buffered by alternative interaction pathways (Thébault and Fontaine, 2010; Stouffer and Bascompte, 2011). Such a configuration allows ecosystems to sustain global stability even when local fluctuations occur, consistent with theories emphasizing modularity, substitutability, and multiple stabilizing routes (MONTOYA and SOLÉ, 2002; Jordán, 2009; Berlow et al., 2009).

From an ecological suitability perspective, this decoupling highlights that structural integration (hyperconnectivity) and dynamic stability (RSA variability) constitute distinct yet complementary dimensions of ecosystem function. Whereas Taylor's Power Law captures the dynamical response of species to environmental fluctuations, hyperconnectivity reflects their potential for information flow and structural embedding within the network. The absence of

a scaling link between these two metrics thus points to a multidimensional stability framework, where ecosystems maintain functional robustness without a direct dependence between structure and dynamics.

Finally, it is important to note that this pattern may partly reflect methodological constraints. Correlation-based networks, as used here, capture undirected co-variation but may obscure causal dependencies. Approaches incorporating bidirectionality—such as Transfer Entropy—have revealed variance-centrality relationships under stronger environmental forcing (Galbraith et al., 2022). Future work integrating causal inference and temporal dynamics could therefore clarify when and how structural and dynamical stability become re-coupled under environmental change.

4.5 Methodological Innovation and Reliability for Ecological Fitness Assessment

Our integrated analytical and computational framework—linking Taylor's Power Law (TPL) with network-based hyperconnectivity (Network Kleiber's Law)—introduces a conceptually and operationally innovative approach to ecosystem fitness assessment. Traditional indicators of ecological conditions often rely on static diversity indices or structural metrics that fail to capture the dynamic interplay between species variability and interaction topology. By combining a scale-invariant descriptor of species dynamics (TPL) with a topological descriptor of network organization (hyperconnectivity), our method bridges this gap and allows the quantitative inference of ecosystem fitness manifesting ecological adaptability to environmental stress across multiple biological hierarchies.

From a methodological standpoint, this framework demonstrates three key advantages. First, it provides cross-scale comparability: TPL and NKL are dimensionless and invariant to sampling scale, enabling integration across taxa, habitats, and time. Second, it enhances diagnostic sensitivity: the covariance between aggregation intensity or organization (ν) and structural centrality metrics (density, clustering, path length) allows early detection of structural optimization or degradation before conventional community indices exhibit significant change. Third, it ensures interpretative transparency, as both components are ecologically interpretable—TPL quantifies behavioral and physiological aggregation responses, while NKL reflects structural embedding and redundancy that regulate abdundance fluctuation. Yet, TPL embeds the complex network structure contained in NKL.

These advantages collectively establish the framework as a robust and transferable diagnostic tool for ecosystem fitness and environmental suitability. The absence of a strict scaling relationship between species variability and structural centrality further supports its reliability: rather than imposing a single deterministic linkage, the approach accommodates context-dependent, multidimensional stability, aligning with real ecological complexity. This flexibility makes it particularly suitable for long-term environmental monitoring, cross-site comparison, and model calibration in systems where both structure and function evolve under anthropogenic and climatic pressures.

5 Conclusions

Facing increasing anthropogenic and climatic pressures on coastal and marine ecosystems, this study aims to move beyond the limitations of conventional biodiversity fitness assessment that rely on macroecological indicators or environmental factors considered independently. Using a multi-marker (12S, 18S, COI) eDNA metabarcoding approach, we compared the systemic community structures between two epitomic site in the Greater Bay Area, China, i.e., Daya Bay and Mirs Bay communities, to construct an integrative quantitative framework that combines co-occurrence species network topology with ecological allometric laws (Taylor's Power Law, TPL, and Network Kleiber's Law, NKL). The two communities are considered as "archetypes" of ecological fitness along "phenotypic" features related to ecological network organization, environme organization, and fluctuations beyond mere species count. This framework was designed to provide new insights into the assessment of ecosystem fitness based on ecological organization and systemic environmental pressure.

Our results revealed contrasting patterns of ecological and environmental organization between the two bay ecosystems, alongside converging eco–environmental patterns within each bay. Daya Bay exhibited higher biodiversity, a larger and more densely connected ecological network, and a relatively even topological structure resembling a small-world configuration. In contrast, Mirs Bay supported a smaller but more hierarchically organized and compartmentalized network, characteristic of a scale-free structure. The environmental network (environe) further highlighted this divergence: Mirs Bay showed a stronger scale-free topology centered on chlorophyll-a at reasonably low concentrations. Conversely, Daya Bay exhibited a more disordered environe rooted in salinity as the central node—reflecting stronger marine dynamics—while chlorophyll-a, although not central, reached high levels associated with elevated nitrate concentrations, consistent with the frequent harmful algal blooms (HABs) reported in the area. This Mirs–Daya Bay dichotomy likely reflects (i) the higher exposure

of Daya Bay communities to the Pearl River Delta effluents, and (ii) the local restoration actions in Mirs Bay, including marine protection, fishing bans, and coral nursery initiatives. Two major findings and one methological innovation stand out.

- First, TPL proved highly informative for ecosystem fitness, where TPL is proportional to species bioomass and depth. TPL provided a strong fit for both ecosystems ($R^2 > 0.86$), with higher fitness ecosystems like the Mirs Bay showing stronger aggregation ($\nu = 1.697$) than lower fitness ecosystems like Daya Bay ($\nu = 1.460$) regardless of specific habitats or trophic scales. Moreover, the TPL exponent (ν) demonstrated strong correlations with both environmental variables (e.g., temperature, $R^2 = 0.85$) and network properties (e.g., network size, $R^2 = 0.97$; centrality, $R^2 = 0.90$), suggesting that it may serve as an integrative systemic indicator linking environmental forcing and ecological network organization. This highlights how ecological networks reflect the organization of environmental networks, where increased randomness in the latter – together with worse levels for each environmental driver – acts as a detrimental factor for the former.

- Second, the decoupling between dynamics and structure was consistently observed in both systems: RSA variability (manifested by the Taylor's law) showed no significant scaling relationship (like the Kleiber's law for communities) with node hyperconnectivity as hypothesized. This might be due to the lack of temporal data, or the correlative network-inference model used, or it can indicate that structural centrality does not necessarily predict species variability. NKL is however showing a more structured bimodal distribution for healthier communities like the Mirs Bay. The results may highlight a context-dependent balance between redundancy and specialization of species (separated by two topological classes as highlighted by two hyperconnectivity classes, that is evident for algae, arthropods, and protists) in maintaining ecosystem resilience.

- Third, methodologically, we introduce a multi-scale diagnostic ecograph framework that integrates the aggregated Taylor's scaling with detailed network topology and species identification. This integration connects the "microscopic" aggregative behavior of species with the "macroscopic" interaction architecture within communities, enabling a systemic assessment of ecosystem function (ecosystemic fitness) that is overcoming the limitations of static biodiversity indices alone such as species richness, and environmental factors considered independently.

Finally, some limitations must be acknowledged. Co-occurrence networks derived from cor-

relation analyses do not necessarily capture direct or causal species interactions. Therefore, simple correlation-based network inference should be used with care when interested in assessing causal interactions. eDNA metabarcoding also faces inherent challenges such as incomplete reference databases and PCR amplification bias, which may affect taxonomic resolution. Furthermore, the present study is based on two bays during a single temporal window; therefore, the generality of the findings should be validated across broader spatial and temporal scales, and in general eDNA sampling requires numerous samples over crirtical ecological corridors for large-scale ecosystems.

Glossary

SR: Shallow Reef, Heart Island, Mirs Bay (∼1.5 m max depth)

CN: Coral Nursery, Heart Island, Mirs Bay (∼2.5 m max depth)

DR: Deep Rocky, Heart Island, Mirs Bay (∼10 m max depth)

RR: Rocky Reef, Heart Island, Mirs Bay (∼2 m max depth)

HO1: Hongshenggong Island site 1, Daya Bay (∼5 m max depth)

HO2: Hongshenggong Island site 2, Daya Bay (∼8 m max depth)

XI: Xiaosanmen Island, Daya Bay (∼10 m max depth)

IL: Ilha Verde Island, Daya Bay (∼ 15 m max depth)

SW: Surface Water

DW: "Deep" Water (intermediate depth)

BO: Bottom Water (from 1.5 to 15 meters depending on the location)

Acknowledgments

Convertino acknowledges support from the Shenzhen Pengcheng Peacock Talents funding (B class, 0020210320), for the project "ECOgeomorphic and Hydroclimatic Impacts on Biodiversity and Ecosystem Function: Mapping Critical Shifts and Connections" (ECOSENSE); the Shenzhen Stability Support Grant (WDZC20231128160214001), "Optimizing Deltas' Natural Engineers: Systemic Restoration to Counter EcoHydroClimate Extremes" (Delta-X); funding from the Shenzhen Science and Technology Program (ZDSYS20220606100806014) for the Shenzhen Key Laboratory of Ecological Remediation and Carbon Sequestration at Tsinghua SIGS; and funding from the Tsinghua SIGS Cross-disciplinary Research and Innovation Fund Research Plan (JC2024011) "The Fibers of Nature: Ecohydrological Flows Assessment via Distributed Fiber-optic Sensing Networks".

Author Contribution

W. Huang performed the calculations, wrote the initial draft of the paper, and created the initial figures. M. Convertino designed and guided the study, provided funding and coordination of the sampling campaign, finalized the figures and completed the final manuscript. W.T. and X.S. were responsible for the eDNA data collection and assisted into the interpretation of results.

Data Availability Statement

All data will be made available in an organized repository in Zenodo.

Competing Interest

The authors declare no competing interests.

Figure Captions

Figure 1. Conceptual scheme of ecograph-envirome nexus for ecosystem fitness assessment. Ecosystems at the macroscale are the bays comprimising the set of habitats considered in the study. Habitats are locations characterized by distinct environmental features (hydrogeomrophic and biogeochemical) (Fig. 2); communities are meso-ecosystems at different depth; populations are OTUs at the family level as a trophic level spanning multiple taxa (molucular markers, i.e. 12S, 18S, and COI). Each taxa or OTU are micro-ecosystem composed by multiple individuals of different or equivalent individuals manifesting collective behavior at different organization. The envirome is the set of hydro-biogeochemical features characterizing the ecosystems.

Figure 2. Map of the study areas, sampling sites, and environmental variables. (A) Location of the two study areas in the eastern waters of Hong Kong. The yellow box indicates the sampling site in Mirs Bay and the red box indicates the site in Daya Bay. (B) Aerial view (by M. Convertino) of the sampling site in Mirs Bay (yellow box in panel A), detailing the four microhabitats: Shallow Reef (SR), Coral Nursery (CN), Deep Rocky (DR), and Rocky Reef (RR). (C) Panoramic view (by M. Convertino) of the sampling site in Daya Bay (red box in panel a), showing the locations of sampling stations HO1, HO2, XI, and IL. put the full name of acronyms for Daya. (D) Environmental factors considered from https://ocean.hkust.edu.hk:8443/SiteMapApi/new/index.jsp with values as year averages considering predicted daily data from 1992.

Figure 3. Relative Species Abundance of samples based on different molecular markers. A, B, and C show the RSA of communities at the family level based on 12S rRNA, 18S rRNA, and COI gene markers, respectively. The vertical axis represents the RSA of each family (%), and the horizontal axis represents different samples, whose names are composed of sampling point-water layer. The Mirs Bay includes four sampling points: CN, DR, RR, and SR sampling points, and the Daya Bay includes HO1, HO2, IL, and XI sampling points. Among these, SW represents surface water, DW represents deep water, and BO represents bottom water. The legend lists the top ten families by relative abundance, with the remaining families of lower RSA grouped under “Others”.

Figure 4. Macroecological local diversity of communities in Mirs Bay and Daya Bay based on three molecular markers. Box plots display species richness (a-c) and the Shannon diversity index (d-f) calculated from OTUs. Diversity metrics are shown for communities identified via the 12S rRNA (a, d), 18S rRNA (b, e), and COI (c, f) genes. Orange and green colors represent samples from Mirs Bay (sites: CN, DR, RR, SR) and Daya Bay (sites: HO1, HO2, IL, XI), respectively.

Figure 5. Co-occurrence networks, key interaction patterns, and four key topological network metrics for communities in Mirs Bay and Daya Bay. (A) Co-occurrence networks for Mirs Bay (left) and Daya Bay (right). Each node represents an OTU, colored by its major taxonomic group (e.g., Algae, Fish, non-algal Protists). Edges indicate significant statistical correlations between OTUs. (B) Proportional distribution of major inter- and intra-group interaction types (e.g., Algae-Algae, Algae-Arthropoda) as a percentage of total network connections. (C) The panels represent Degree, Average Path Length, Betweenness Centrality, and Clustering Coefficient from top-left to bottom-right.

Figure 6. Taylor's Power Law and Network Kleiber's of species variance-mean and hyperconnectivity. (A and B) The logscale relationship between RSA mean and variance in Mirs Bay and Daya Bay is shown. The slope of the fitted regression line represents the TPL exponent ν, which quantifies the degree of aggregation that is increasing with biomass and depth. (C and D) show the logscale relationship between hyperconnectivity and abundance variance (NKL), with an assumed scaling low that does not support the hypothesis of scaling due to the strong bimodality of OTU distribution for all taxa. Each point represents a taxon, color-coded by functional type—Algae, Arthropods, Fish, Fungi, Mollusks, Other Animals, Non-algal Protists, and Unclassified groups.

Figure 7. Envirome-Ecograph correlation networks, and sensitivity of Taylor's Power Law Exponent (TPL) to key environmental factors in Mirs Bay and Daya Bay. (A and B) The matrix shows Spearman correlations (r) between environmental factors, with color intensity indicating strength and symbols denoting significance ($*, p < 0.05$; $**, p < 0.01$; $***, p < 0.001$). The network displays Mantel correlations between communities and environmental factors, with line thickness representing r and color indicating significance. (C) Assumed linear relationships between the TPL exponent and five key marine environmental variables: chlorophyll-a, nitrate, dissolved oxygen, salinity, and temperature. Each

point represents an individual sample. Colors distinguish sample origins (red: Mirs Bay; teal: Daya Bay), while shapes indicate sampling depths (circle: surface; triangle: deep; square: bottom). Dashed lines represent linear regression fits, with shaded gray areas indicating the 95% confidence intervals. Regression equations, coefficients of determination (R^2), and significance levels (P-values) are annotated within each subplot.

References

Sean C. Anderson, Andrew B. Cooper, and Nicholas K. Dulvy. Ecological prophets: quantifying metapopulation portfolio effects. Methods in Ecology and Evolution, 4(10):971–981, 2013. doi: https://doi.org/10.1111/2041-210X.12093. URL https://besjournals.onlinelibrary.wiley.com/doi/abs/10.1111/2041-210X.12093.

Albert Barberán, Scott T Bates, Emilio O Casamayor, and Noah Fierer. Using network analysis to explore co-occurrence patterns in soil microbial communities. The ISME journal, 6(2):343–351, 2012.

Edward B Barbier, Sally D Hacker, Chris Kennedy, Evamaria W Koch, Adrian C Stier, and Brian R Silliman. The value of estuarine and coastal ecosystem services. Ecological monographs, 81(2):169–193, 2011.

Jordi Bascompte and Pedro Jordano. Plant-animal mutualistic networks: The architecture of biodiversity. Annual Review of Ecology, Evolution, and Systematics, 38(1):567–593, 2007.

Eric L. Berlow, Jennifer A. Dunne, Neo D. Martinez, Philip B. Stark, Richard J. Williams, and Ulrich Brose. Simple prediction of interaction strengths in complex food webs. Proceedings of the National Academy of Sciences, 106(1):187–191, January 2009. ISSN 1091-6490. doi: 10.1073/pnas.0806823106.

David Berry and Stefanie Widder. Deciphering microbial interactions and detecting keystone species with co-occurrence networks. Frontiers in microbiology, 5:219, 2014.

Rosetta C Blackman, Hsi-Cheng Ho, Jean-Claude Walser, and Florian Altermatt. Spatiotemporal patterns of multi-trophic biodiversity and food-web characteristics uncovered across a river catchment using environmental DNA. Communications Biology, 5(1):259, 2022.

Guogui Chen, Wenqing Wang, Yi Liu, Yamian Zhang, Wei Ma, Kun Xin, and Mao Wang. Uncovering the relative influences of space and environment in shaping the biogeographic patterns of mangrove mollusk diversity. ICES Journal of Marine Science, 77(1):30–39, 2019.

Matthew R. D. Cobain, Markus Brede, and Clive N. Trueman. Taylor's power law captures the effects of environmental variability on community structure: An example from fishes in the north sea. Journal of Animal Ecology, 88(2):290–301, 2018a.

Matthew R. D. Cobain, Markus Brede, and Clive N. Trueman. Taylor's power law captures the effects of environmental variability on community structure: An example from fishes in the north sea. Journal of Animal Ecology, 88(2):290–301, 2018b.

Joel E Cohen, Meng Xu, and William SF Schuster. Stochastic multiplicative population growth predicts and interprets taylor's power law of fluctuation scaling. Proceedings of the Royal Society B: Biological Sciences, 280(1757):20122955, 2013.

Harrison T Coleman, Ty G Matthews, Craig DH Sherman, Owen J Holland, Zach SR Clark, Lachlan Farrington, Gavin Prentice, and Adam D Miller. Contrasting patterns of biodiversity across wetland habitats using single-time-point environmental DNA surveys. Aquatic Conservation: Marine and Freshwater Ecosystems, 33(12):1401–1412, 2023.

Matteo Convertino. Space sculpts time: Metacommunity risk and resilience. Ecological Indicators, 178:113819, 2025a.

Matteo Convertino. Space sculpts time: Metacommunity risk and resilience. Ecological Indicators, 178:113819, 2025b.

Matteo Convertino, Yuhan Wu, and Hui Dong. Baselining urban ecosystems from sentinel species: Fitness, flows, and sinks. Entropy, 27(5):486, 2025.

Gábor Csárdi and Tamás Nepusz. The igraph software package for complex network research. InterJournal, Complex Systems(1695):1–9, 2006.

Kristy Deiner, Holly M Bik, Elvira Mächler, Mathew Seymour, Anaïs Lacoursière-Roussel, Florian Altermatt, Simon Creer, Iliana Bista, David M Lodge, Natasha De Vere, et al. Environmental DNA metabarcoding: Transforming how we survey animal and plant communities. Molecular ecology, 26(21):5872–5895, 2017.

Eva Delmas, Mathilde Besson, Marie-Hélène Brice, Laura A. Burkle, Giulio V. Dalla Riva, Marie-Josée Fortin, Dominique Gravel, Paulo R. Guimarães, David H. Hembry, Erica A. Newman, Jens M. Olesen, Mathias M. Pires, Justin D. Yeakel, and Timothée Poisot. Analysing ecological networks of species interactions. Biological Reviews, 94(1):16–36, 2018.

Ye Deng, Yi-Huei Jiang, Yunfeng Yang, Zhili He, Feng Luo, and Jizhong Zhou. Molecular ecological network analyses. BMC bioinformatics, 13(1):113, 2012.

Ethan R. Deyle, Robert M. May, Stephan B. Munch, and George Sugihara. Tracking and forecasting ecosystem interactions in real time. Proceedings of the Royal Society B: Biological Sciences, 283(1822):20152258, 2016.

Caoyun Diao, Hui Jia, Shujin Guo, Gang Hou, Weiwei Xian, and Hui Zhang. Biodiversity exploration in autumn using environmental DNA in the south china sea. Environmental Research, 204:112357, 2022.

Anni Djurhuus, Jesse Port, Collin J Closek, Kevan M Yamahara, Ofelia Romero-Maraccini, Kristine R Walz, Dawn B Goldsmith, Reiko Michisaki, Mya Breitbart, Alexandria B Boehm, et al. Evaluation of filtration and DNA extraction methods for environmental DNA biodiversity assessments across multiple trophic levels. Frontiers in Marine Science, 4:314, 2017.

Anni Djurhuus, Collin J Closek, Ryan P Kelly, Kathleen J Pitz, Reiko P Michisaki, Hilary A Starks, Kristine R Walz, Elizabeth A Andruszkiewicz, Emily Olesin, Katherine Hubbard, et al. Environmental DNA reveals seasonal shifts and potential interactions in a marine community. Nature Communications, 11(1):254, 2020.

Scott C Doney, Mary Ruckelshaus, J Emmett Duffy, James P Barry, Francis Chan, Chad A English, Heather M Galindo, Jacqueline M Grebmeier, Anne B Hollowed, Nancy Knowlton, et al. Climate change impacts on marine ecosystems. Annual review of marine science, 4 (2012):11–37, 2012.

Jennifer A. Dunne, Richard J. Williams, and Neo D. Martinez. Food-web structure and network theory: The role of connectance and size. Proceedings of the National Academy of Sciences, 99(20):12917, 2002.

Robert C. Edgar. Search and clustering orders of magnitude faster than blast. Bioinformatics, 26(19):2460, 2010.

Zeynep Ersoy, Meritxell Abril, Miguel Cañedo-Argüelles, Carmen Espinosa, Lidia Vendrell-Puigmitja, and Lorenzo Proia. Experimental assessment of salinization effects on freshwater zooplankton communities and their trophic interactions under eutrophic conditions. Environmental Pollution, 313:120127, 2022.

Patrick Eskuche-Keith, Simeon L Hill, Philip Hollyman, Michelle L Taylor, and Eoin J O'Gorman. Trophic structuring of modularity alters energy flow through marine food webs. Frontiers in Marine Science, 9:1046150, 2023.

Santo Fortunato. Community detection in graphs. Physics reports, 486(3-5):75–174, 2010.

Mara A Freilich, Evie Wieters, Bernardo R Broitman, Pablo A Marquet, and Sergio A Navarrete. Species co-occurrence networks: can they reveal trophic and non-trophic interactions in ecological communities? Ecology, 99(3):690–699, 2018.

Jonathan Friedman, Eric J. Alm, and Christian Von Mering. Inferring correlation networks from genomic survey data. Plos Computational Biology, 8(9):e1002687, 2012.

Elroy Galbraith, P.R. Frade, and Matteo Convertino. Metabolic shifts of oceans: Summoning bacterial interactions. Ecological Indicators, 138:108871, May 2022.

Douglas S. Glazier. Is metabolic rate a universal 'pacemaker' for biological processes? Biological Reviews, 90(2):377–407, 2014.

Benjamin S Halpern, Shaun Walbridge, Kimberly A Selkoe, Carrie V Kappel, Fiorenza Micheli, Caterina d'Agrosa, John F Bruno, Kenneth S Casey, Colin Ebert, Helen E Fox, et al. A global map of human impact on marine ecosystems. Science, 319(5865):948–952, 2008.

John Harte, Micah Brush, Erica A Newman, and Kaito Umemura. An equation of state unifies diversity, productivity, abundance and biomass. Communications biology, 5(1):874, 2022.

Rheyda Hinlo, Dianne Gleeson, Mark Lintermans, and Elise Furlan. Methods to maximise recovery of environmental DNA from water samples. PLOS ONE, 12(6):e0179251, 2017.

Dongwei Hou, Zhijian Huang, Shenzheng Zeng, Jian Liu, Dongdong Wei, Xisha Deng, Shaoping Weng, Zhili He, and Jianguo He. Environmental factors shape water microbial community structure and function in shrimp cultural enclosure ecosystems. Frontiers in microbiology, 8:2359, 2017.

Richard K. Johnson and David G. Angeler. Effects of agricultural land use on stream assemblages: Taxon-specific responses of alpha and beta diversity. Ecological Indicators, 45: 386–393, 2014.

J. Iwan Jones, Amanda Arnold, Dominik Buchner, John F. Murphy, Jasmine N. Childress, Pedro Beja, Florian Altermatt, Kristian Meissner, Ian Adams, and Meri Anderson. Sources of uncertainty in dna metabarcoding of whole communities: Implications for its use in biomonitoring. Methods in Ecology and Evolution, 16(8):1658–1673, 2025.

Ferenc Jordán. Keystone species and food webs. Philosophical Transactions of the Royal Society B: Biological Sciences, 364(1524):1733–1741, June 2009. ISSN 1471-2970. doi: 10.1098/rstb.2008.0335.

Mark Kac. Can one hear the shape of a drum? The american mathematical monthly, 73 (4P2):1–23, 1966.

AM Kilpatrick and AR Ives. Species interactions can explain taylor's power law for ecological time series. Nature, 422(6927):65–68, 2003.

Max Kleiber. Body size and metabolic rate. Physiological reviews, 27(4):511–541, 1947.

Girish Kumar, Ashley M Reaume, Emily Farrell, and Michelle R Gaither. Comparing eDNA metabarcoding primers for assessing fish communities in a biodiverse estuary. PloS one, 17(6):e0266720, 2022.

Pietro Landi, Henintsoa O Minoarivelo, Åke Brännström, Cang Hui, and Ulf Dieckmann. Complexity and stability of ecological networks: a review of the theory. Population ecology, 60(4):319–345, 2018.

Matthieu Leray and Nancy Knowlton. DNA barcoding and metabarcoding of standardized samples reveal patterns of marine benthic diversity. Proceedings of the National Academy of Sciences, 112(7):2076–81, 2015.

Jianlong Li, Lori-Jayne Lawson Handley, Daniel S. Read, and Bernd Hänfling. The effect of filtration method on the efficiency of environmental DNA capture and quantification via metabarcoding. Molecular Ecology Resources, 18(5):1102–1114, 2018.

Jie Li and Matteo Convertino. Optimal microbiome networks: Macroecology and criticality. Entropy, 21(5):506, 2019. doi: 10.3390/e21050506.

Lee Hsiang Liow, Leigh Van Valen, and Nils Chr Stenseth. Red queen: from populations to taxa and communities. Trends in ecology & evolution, 26(7):349–358, 2011.

Pablo A. Marquet, Renato A. Quinones, Sebastian Abades, Fabio Labra, Marcelo Tognelli, Matias Arim, and Marcelo Rivadeneira. Scaling and power-laws in ecological systems. Journal of Experimental Biology, 208(9):1749–1769, May 2005. ISSN 0022-0949. doi: 10.1242/jeb.01588.

Kevin Shear McCann. The diversity–stability debate. Nature, 405(6783):228–233, 2000.

Ewa Merz, Erik Saberski, Luis J. Gilarranz, Peter D. F. Isles, George Sugihara, Christine Berger, and Francesco Pomati. Disruption of ecological networks in lakes by climate change and nutrient fluctuations. Nature Climate Change, 13(4):389–396, 2023.

Wen Jye Mok, Mazlan Abd Ghaffar, Mohd Iqbal Mohd Noor, Fathurrahman Lananan, and Mohamad Nor Azra. Understanding climate change and heavy metals in coastal areas: A macroanalysis assessment. Water, 15(5):891, 2023.

JOSE M. MONTOYA and RICARD V. SOLÉ. Small world patterns in food webs. Journal of Theoretical Biology, 214(3):405–412, 2002.

José M. Montoya, Stuart L. Pimm, and Ricard V. Solé. Ecological networks and their fragility. Nature, 442(7100):259–264, July 2006.

Bryan N Nguyen, Elaine W Shen, Janina Seemann, Adrienne MS Correa, James L O'Donnell, Andrew H Altieri, Nancy Knowlton, Keith A Crandall, Scott P Egan, W Owen McMillan, et al. Environmental DNA survey captures patterns of fish and invertebrate diversity across a tropical seascape. Scientific reports, 10(1):6729, 2020.

Jari Oksanen, F. Guillaume Blanchet, Michael Friendly, Roeland Kindt, Pierre Legendre, Dan McGlinn, Peter R. Minchin, R. B. O'Hara, Gavin L. Simpson, Peter Solymos, M. Henry H. Stevens, Eduard Szöecs, and Helene Wagner. vegan: Community Ecology Package, 2022. URL https://CRAN.R-project.org/package=vegan. R package version 2.6-4.

Jens M Olesen, Jordi Bascompte, Yoko L Dupont, and Pedro Jordano. The modularity of pollination networks. Proceedings of the National Academy of Sciences, 104(50):19891–19896, 2007.

Prajwal Padmanabha, Giorgio Nicoletti, Davide Bernardi, Samir Suweis, Sandro Azaele, Andrea Rinaldo, and Amos Maritan. Landscape and environmental heterogeneity support coexistence in competitive metacommunities. Proceedings of the National Academy of Sciences, 121(44), 2024.

Juan J Pierella Karlusich, Karen Cosnier, Lucie Zinger, Nicolas Henry, Charlotte Nef, Guillaume Bernard, Eleonora Scalco, Etienne Dvorak, Fabio Rocha Jimenez Vieira, et al. Patterns and drivers of diatom diversity and abundance in the global ocean. Nature Communications, 16(1):3452, 2025.

Landi Pietro, Henintsoa O. Minoarivelo, Åke Brännström, Hui Cang, and Dieckmann Ulf. Complexity and stability of ecological networks: a review of the theory. Population Ecology, 2018.

Jens O Riede, Bjrn C Rall, Carolin Banasek-Richter, Sergio A Navarrete, and Ulrich Brose. Scaling of food-web properties with diversity and complexity across ecosystems. Advances in Ecological Research, 42:139–170, 2010.

Sakib Tahmid Rishan, Richard J Kline, and Md Saydur Rahman. Applications of environmental DNA (eDNA) to detect subterranean and aquatic invasive species: A critical review

on the challenges and limitations of eDNA metabarcoding. Environmental Advances, 12: 100370, 2023.

Tanya L Rogers, Samuel M Bashevkin, Christina E Burdi, Denise D Colombano, Peter N Dudley, Brian Mahardja, Lara Mitchell, Sarah Perry, and Parsa Saffarinia. Evaluating top-down, bottom-up, and environmental drivers of pelagic food web dynamics along an estuarine gradient. Ecology, 105(4):e4274, 2024.

Torbjørn Rognes, Tomáš Flouri, Ben Nichols, Christopher Quince, and Frédéric Mahé. Vsearch: a versatile open source tool for metagenomics. PeerJ, 4:e2584, 2016.

Till Röthig, Stacey M Trevathan-Tackett, Christian R Voolstra, Cliff Ross, Samuel Chaffron, Paul J Durack, Laura M Warmuth, and Michael Sweet. Human-induced salinity changes impact marine organisms and ecosystems. Global Change Biology, 29(17):4731–4749, 2023.

Krista M. Ruppert, Richard J. Kline, and Md Saydur Rahman. Past, present, and future perspectives of environmental DNA (eDNA) metabarcoding: A systematic review in methods, monitoring, and applications of global eDNA. Global Ecology and Conservation, 17: e00547, 2019.

Joseph L. Servadio and Matteo Convertino. Optimal information networks: Application for data-driven integrated health in populations. Science Advances, 4(2), 2018. doi: 10.1126/sciadv.1701088.

Johan Spens, Alice R. Evans, David Halfmaerten, Steen W. Knudsen, Mita E. Sengupta, Sarah S. T. Mak, Eva E. Sigsgaard, and Micaela Hellström. Comparison of capture and storage methods for aqueous macrobial DNA using an optimized extraction protocol: advantage of enclosed filter. Methods in Ecology and Evolution, 8(5):635–645, 2016.

Daniel B. Stouffer and Jordi Bascompte. Compartmentalization increases food-web persistence. Proceedings of the National Academy of Sciences, 108(9):3648–3652, February 2011.

Lionel Roy Taylor. Aggregation, variance and the mean. Nature, 189(4766):732–735, 1961.

The Hong Kong University of Science and Technology. HKUST(GZ) Marine and Atmospheric Environment Monitoring System. https://ocean.ust.hk:8443/SiteMapApi/new/index.jsp, 2025. Accessed: 2025-06-15.

Ross M. Thompson, Ulrich Brose, Jennifer A. Dunne, Robert O. Hall, Sally Hladyz, Roger L. Kitching, Neo D. Martinez, Heidi Rantala, Tamara N. Romanuk, Daniel B. Stouffer, and Jason M. Tylianakis. Food webs: reconciling the structure and function of biodiversity. Trends in Ecology & Evolution, 27(12):689–697, 2012.

Philip Francis Thomsen and Eske Willerslev. Environmental DNA–an emerging tool in conservation for monitoring past and present biodiversity. Biological conservation, 183:4–18, 2015.

Elisa Thébault and Colin Fontaine. Stability of ecological communities and the architecture of mutualistic and trophic networks. Science, 329(5993):853–856, 2010.

Ewan Trégarot, Juan Pablo D'Olivo, Andrea Zita Botelho, Andrea Cabrito, Gabriel O Cardoso, Gema Casal, Cindy C Cornet, Simon M Cragg, A Karima Degia, Stein Fredriksen, et al. Effects of climate change on marine coastal ecosystems–a review to guide research and management. Biological Conservation, 289:110394, 2024.

Stacey M. Trevathan-Tackett, Craig D.H. Sherman, Megan J. Huggett, Alexandra H. Campbell, Bonnie Laverock, Valentina Hurtado-McCormick, Justin R. Seymour, Alana Firl, Lauren F. Messer, Tracy D. Ainsworth, Karita L. Negandhi, Daniele Daffonchio, Suhelen Egan, Aschwin H. Engelen, Marco Fusi, Torsten Thomas, Laura Vann, Alejandra Hernandez-Agreda, Han Ming Gan, Ezequiel M. Marzinelli, Peter D. Steinberg, Leo Hardtke, and Peter I. Macreadie. A horizon scan of priorities for coastal marine microbiome research. Nature Ecology & Evolution, 3(11):1509–1520, 2019.

DIEGO P. VÁZQUEZ, ROBERT POULIN, BORIS R. KRASNOV, and GEORGY I. SHENBROT. Species abundance and the distribution of specialization in host–parasite interaction networks. Journal of Animal Ecology, 74(5):946–955, September 2005.

Haojiong Wang and Matteo Convertino. Algal bloom ties: Systemic biogeochemical stress and chlorophyll-a shift forecasting. Ecological Indicators, 154:110760, 2023a. doi: 10.1016/j.ecolind.2023.110760.

Haojiong Wang and Matteo Convertino. Algal bloom ties: Systemic biogeochemical stress and chlorophyll-a shift forecasting. Ecological Indicators, 154:110760, 2023b.

Haojiong Wang, Elroy Galbraith, and Matteo Convertino. Algal bloom ties: Spreading network inference and extreme eco-environmental feedback. Entropy, 25(4):636, 2023. doi: 10.3390/e25040636.

Kirk O. Winemiller, Eric R. Pianka, Laurie J. Vitt, and Anthony Joern. Food web laws or niche theory? six independent empirical tests. The American Naturalist, 158(2):193–199, 2001.

Boris Worm, Edward B Barbier, Nicola Beaumont, J Emmett Duffy, Carl Folke, Benjamin S

Halpern, Jeremy BC Jackson, Heike K Lotze, Fiorenza Micheli, Stephen R Palumbi, et al. Impacts of biodiversity loss on ocean ecosystem services. Science, 314(5800):787–790, 2006.

Feng-Xia Wu, Yang-Guang Gu, Qing-Xia Liu, Shu-Fei Zhang, Yi-Yong Rao, Hua-Xue Liu, Ming Dai, Yan-Guo Wang, and Hong-Hui Huang. Research on the seasonal variation of zooplankton community in daya bay, south china sea. Frontiers in Marine Science, 10, 2023.

Lirong Wu and Matteo Convertino. Ecological corridor design for ecoclimatic regulation: Species as eco-engineers. Ecological Indicators, 171:113149, 2025.

Helen F Yan, Renato A Morais, and David R Bellwood. Species abundances surpass richness effects in the biodiversity-ecosystem function relationship across marine fishes. Nature Communications, 16(1):7789, 2025.

Li-Juan Yang, Ya Tao, Xia Jiang, Ying Wang, Ye-Hao Li, Long Zhou, Pu-Ze Wang, Yuan-Yuan Li, Xu Zhao, Hai-Jun Wang, et al. Interactive effects of nutrients and salinity on zooplankton in subtropical plateau lakes with contrasting water depth. Frontiers in Environmental Science, 11:1110746, 2023.

Meng Yao, Shan Zhang, Qi Lu, Xiaoyu Chen, Si-Yu Zhang, Yueqiao Kong, and Jindong Zhao. Fishing for fish environmental DNA: Ecological applications, methodological considerations, surveying designs, and ways forward. Molecular ecology, 31(20):5132–5164, 2022.

Hanxiao Zhang, Shouliang Huo, Yong Liu, Jingtian Zhang, Yi Li, Peilian Zhang, Jing Wang, Weihui Huang, and Nanyan Weng. Multiple stressors drive multitrophic biodiversity and ecological network dynamics in a shrinking sandy lake. Communications Earth & Environment, 5(1), 2024a.

Jiang Zhang and Liangpeng Guo. Scaling behaviors of weighted food webs as energy transportation networks. Journal of Theoretical Biology, 264(3):760–770, 2010.

Jiaqi Zhang and Matteo Convertino. Blueprinting the ecosystem health index for blue carbon ecotones. IScience, 27(12), 2024.

Jiaqi Zhang and Matteo Convertino. Novel functional drainage density for blue carbon ecotones. Ecological Indicators, 174:113385, 2025.

Zhenyan Zhang, Qi Zhang, Bingfeng Chen, Yitian Yu, Tingzhang Wang, Nuohan Xu, Xiaoji Fan, Josep Penuelas, Zhengwei Fu, Ye Deng, et al. Global biogeography of microbes driving ocean ecological status under climate change. Nature communications, 15(1):4657, 2024b.

Indrė Žliobaitė. Laws of macroevolutionary expansion. Proceedings of the National Academy of Sciences, 121(33):e2314694121, 2024.

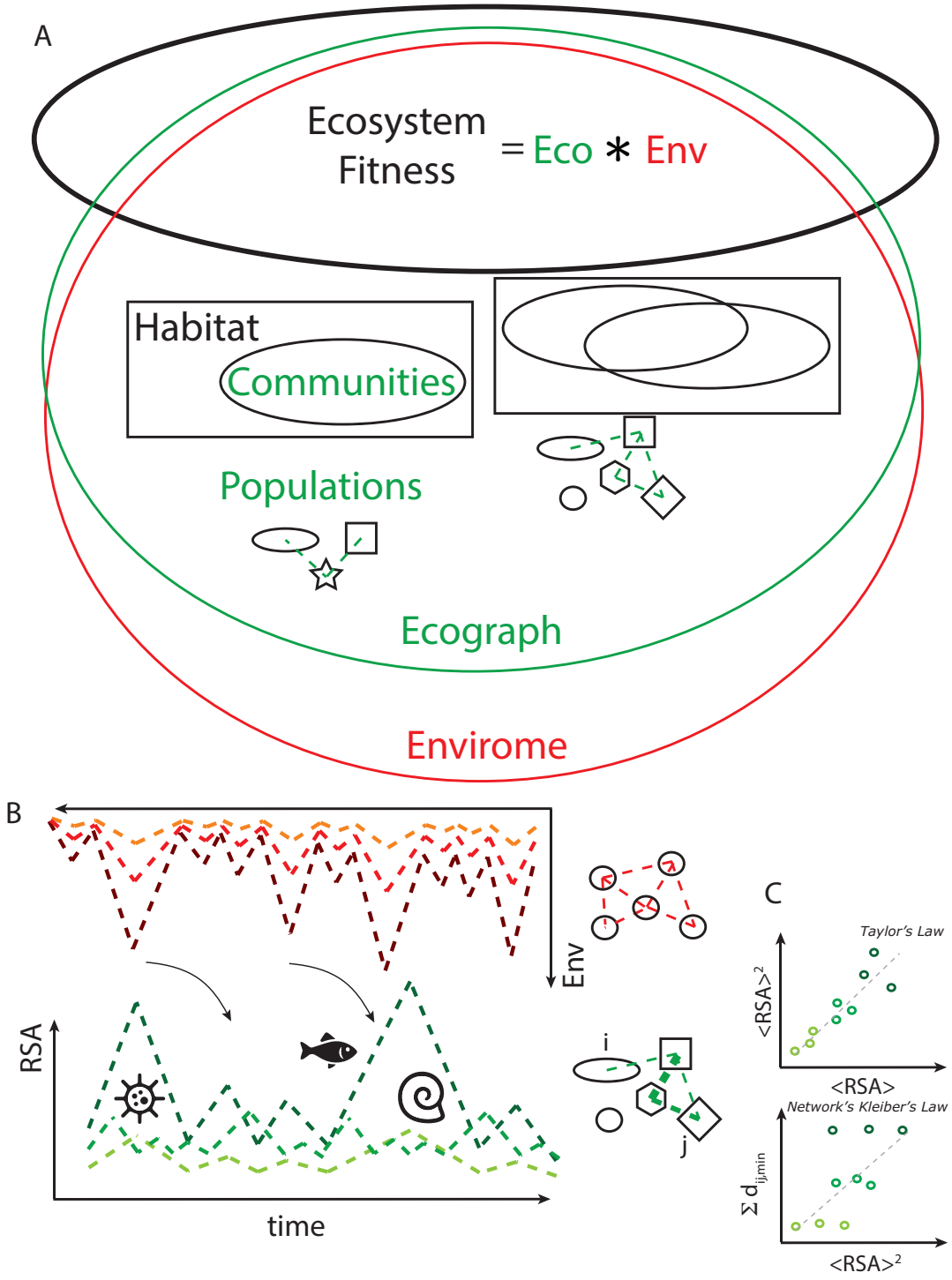

A
Ecosystem Fitness
= Eco * Env
Habitat
Communities
Populations
Ecograph
Envirome
B
RSA
time
Env
i
j
C
Taylor's Law
<RSA>²
<RSA>
Network's Kleiber's Law
Σ d ij,min
<RSA>²

Figure 1:

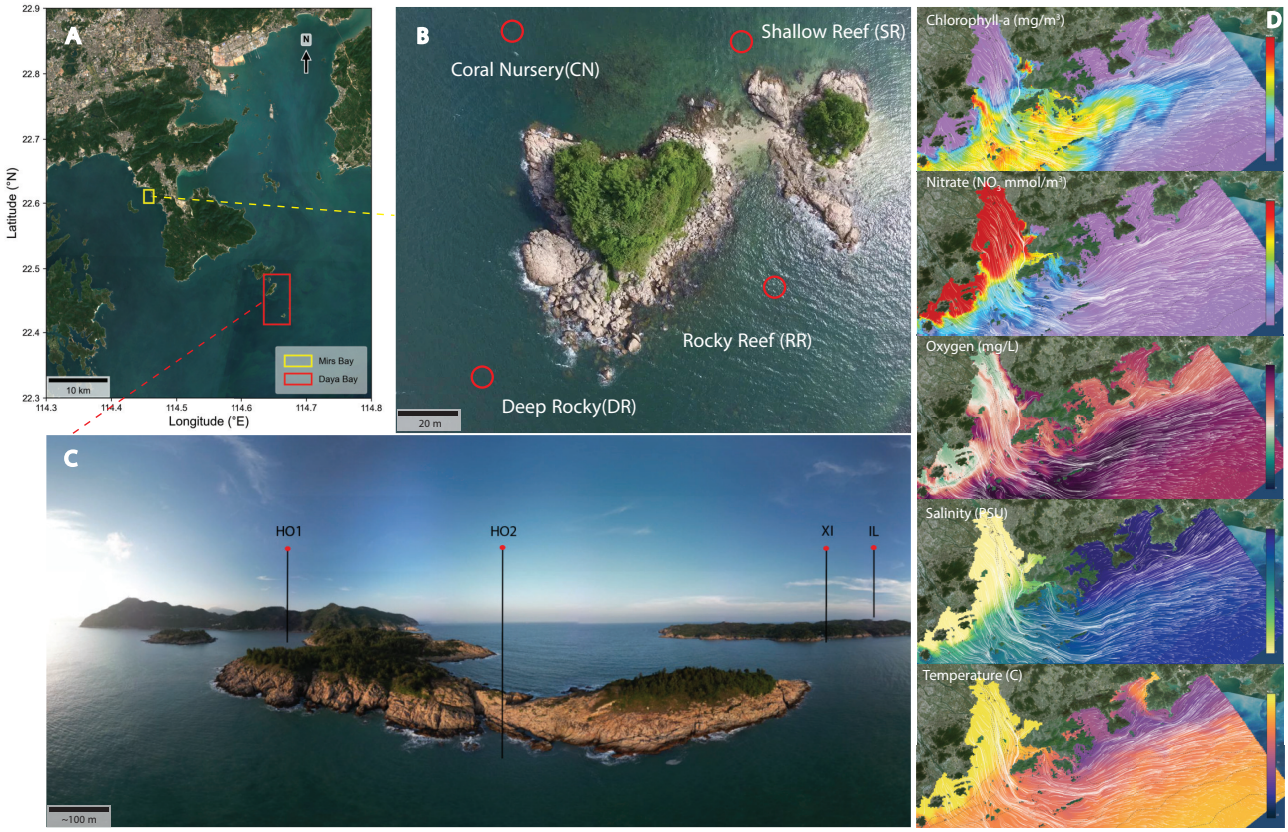

A
B
C
D
Latitude (°N)
Longitude (°E)
22.9
22.8
22.7
22.6
22.5
22.4
22.3
114.3
114.4
114.5
114.6
114.7
114.8
N
10 km
Mirs Bay
Daya Bay
Coral Nursery(CN)
Shallow Reef (SR)
Rocky Reef (RR)
Deep Rocky(DR)
20 m
HO1
HO2
XI
IL
~100 m
Chlorophyll-a (mg/m³)
Nitrate (NO₃ mmol/m³)
Oxygen (mg/L)
Salinity (PSU)
Temperature (C)

Figure 2:

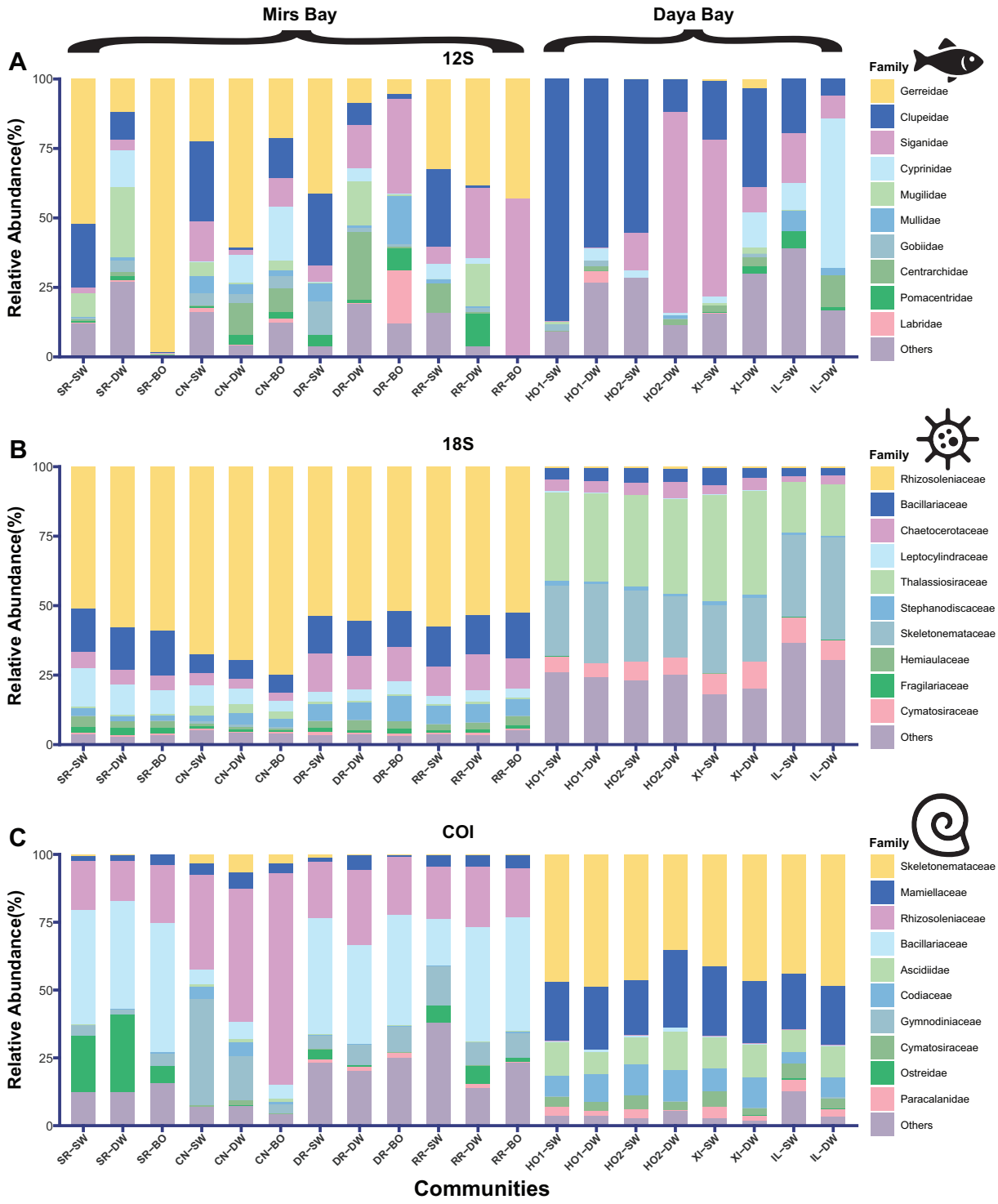

Mirs Bay
Daya Bay
A
12S
Relative Abundance(%)
100
75
50
25
0
SR-SW
SR-DW
SR-BO
CN-SW
CN-DW
CN-BO
DR-SW
DR-DW
DR-BO
RR-SW
RR-DW
RR-BO
HO1-SW
HO1-DW
HO2-SW
HO2-DW
XI-SW
XI-DW
IL-SW
IL-DW
Family
Gerreidae
Clupeidae
Siganidae
Cyprinidae
Mugilidae
Mullidae
Gobiidae
Centrarchidae
Pomacentridae
Labridae
Others
B
18S
Relative Abundance(%)
Family
Rhizosoleniaceae
Bacillariaceae
Chaetocerotaceae
Leptocylindraceae
Thalassiosiraceae
Stephanodiscaceae
Skeletonemataceae
Hemiaulaceae
Fragilariaceae
Cymatosiraceae
Others
C
COI
Relative Abundance(%)
Family
Skeletonemataceae
Mamiellaceae
Rhizosoleniaceae
Bacillariaceae
Ascidiidae
Codiaceae
Gymnodiniaceae
Cymatosiraceae
Ostreidae
Paracalanidae
Others
Communities

Figure 3:

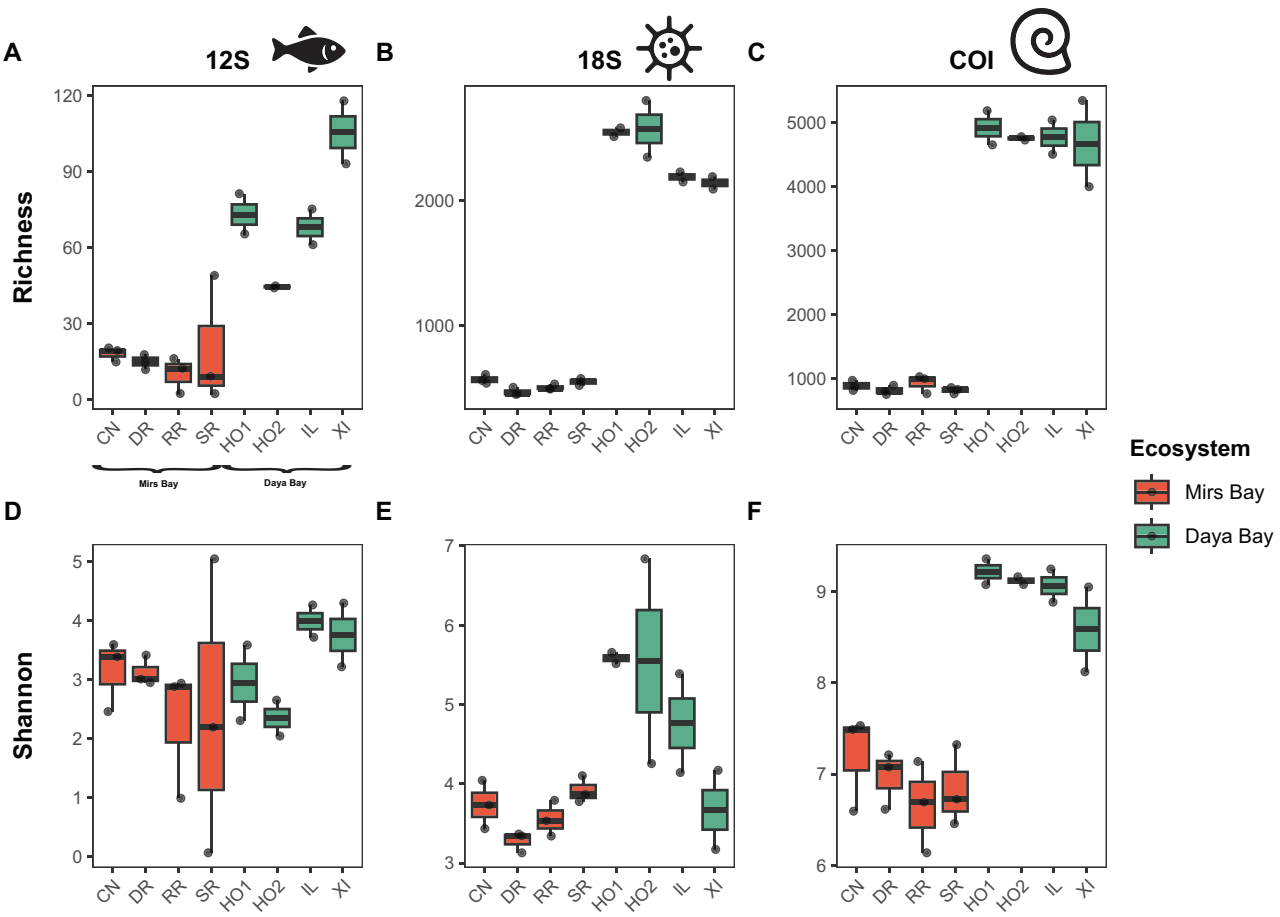

A
12S
B
18S
C
COI
Richness
Shannon
CN
DR
RR
SR
HO1
HO2
IL
XI
Mirs Bay
Daya Bay
Ecosystem
Mirs Bay
Daya Bay

Figure 4:

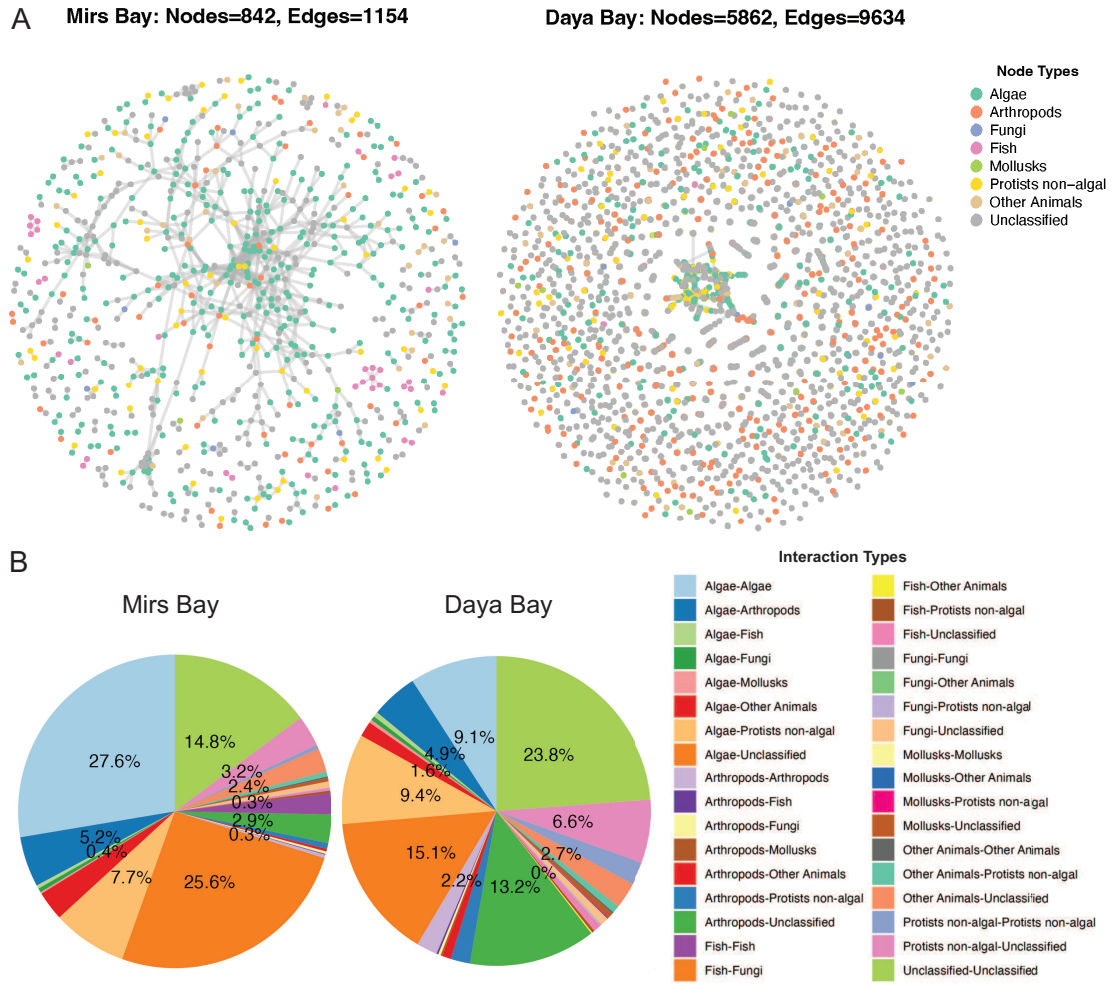

A
Mirs Bay: Nodes=842, Edges=1154
Daya Bay: Nodes=5862, Edges=9634
Node Types
Algae
Arthropods
Fungi
Fish
Mollusks
Protists non−algal
Other Animals
Unclassified
B
Mirs Bay
Daya Bay
27.6%
14.8%
3.2%
2.4%
0.3%
2.9%
0.3%
5.2%
0.4%
7.7%
25.6%
9.1%
23.8%
4.9%
1.6%
9.4%
6.6%
2.7%
0%
15.1%
2.2%
13.2%
Interaction Types
Algae-Algae
Algae-Arthropods
Algae-Fish
Algae-Fungi
Algae-Mollusks
Algae-Other Animals
Algae-Protists non-algal
Algae-Unclassified
Arthropods-Arthropods
Arthropods-Fish
Arthropods-Fungi
Arthropods-Mollusks
Arthropods-Other Animals
Arthropods-Protists non-algal
Arthropods-Unclassified
Fish-Fish
Fish-Fungi
Fish-Other Animals
Fish-Protists non-algal
Fish-Unclassified
Fungi-Fungi
Fungi-Other Animals
Fungi-Protists non-algal
Fungi-Unclassified
Mollusks-Mollusks
Mollusks-Other Animals
Mollusks-Protists non-agal
Mollusks-Unclassified
Other Animals-Other Animals
Other Animals-Protists non-algal
Other Animals-Unclassified
Protists non-algal-Protists non-algal
Protists non-algal-Unclassified
Unclassified-Unclassified
C
Probability Density Function
Degree
0.020
0.015
0.010
0.005
0.000
0
500
1000
1500
Average Path Length
Ecosystem
Daya Bay
Mirs Bay
6
4
2
0
1
2
3
4
Betweenness Centrality
3e−04
2e−04
1e−04
0e+00
0e+00
5e+04
1e+05
Clustering Coefficient
30
20
10
0
0.00
0.25
0.50
0.75
1.00

Figure 5:

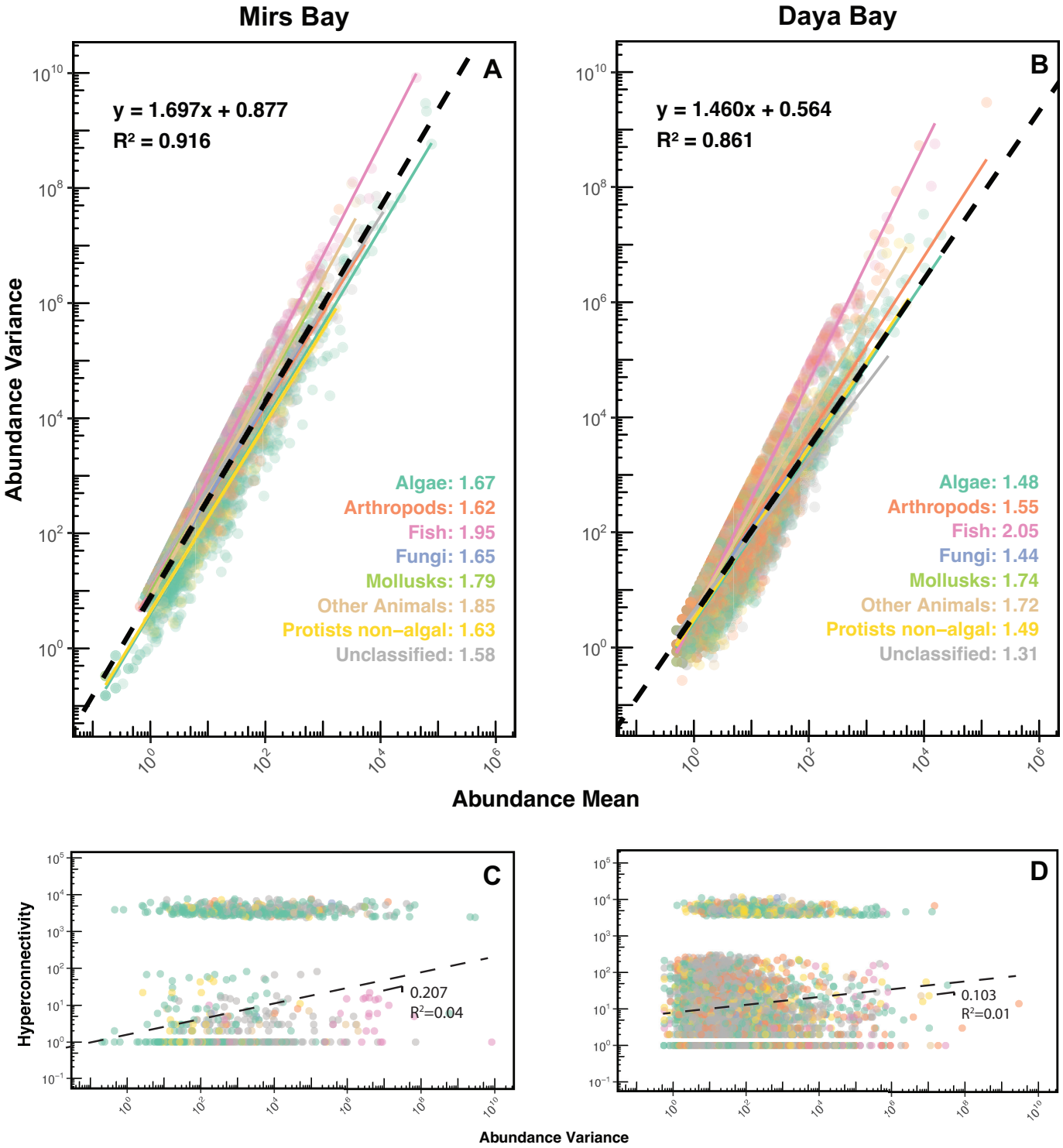

Mirs Bay
Daya Bay
A
B
y = 1.697x + 0.877
R² = 0.916
y = 1.460x + 0.564
R² = 0.861
Abundance Variance
Abundance Mean
Algae: 1.67
Arthropods: 1.62
Fish: 1.95
Fungi: 1.65
Mollusks: 1.79
Other Animals: 1.85
Protists non−algal: 1.63
Unclassified: 1.58
Algae: 1.48
Arthropods: 1.55
Fish: 2.05
Fungi: 1.44
Mollusks: 1.74
Other Animals: 1.72
Protists non−algal: 1.49
Unclassified: 1.31
C
D
Hyperconnectivity
0.207
R²=0.04
0.103
R²=0.01
Abundance Variance

Figure 6:

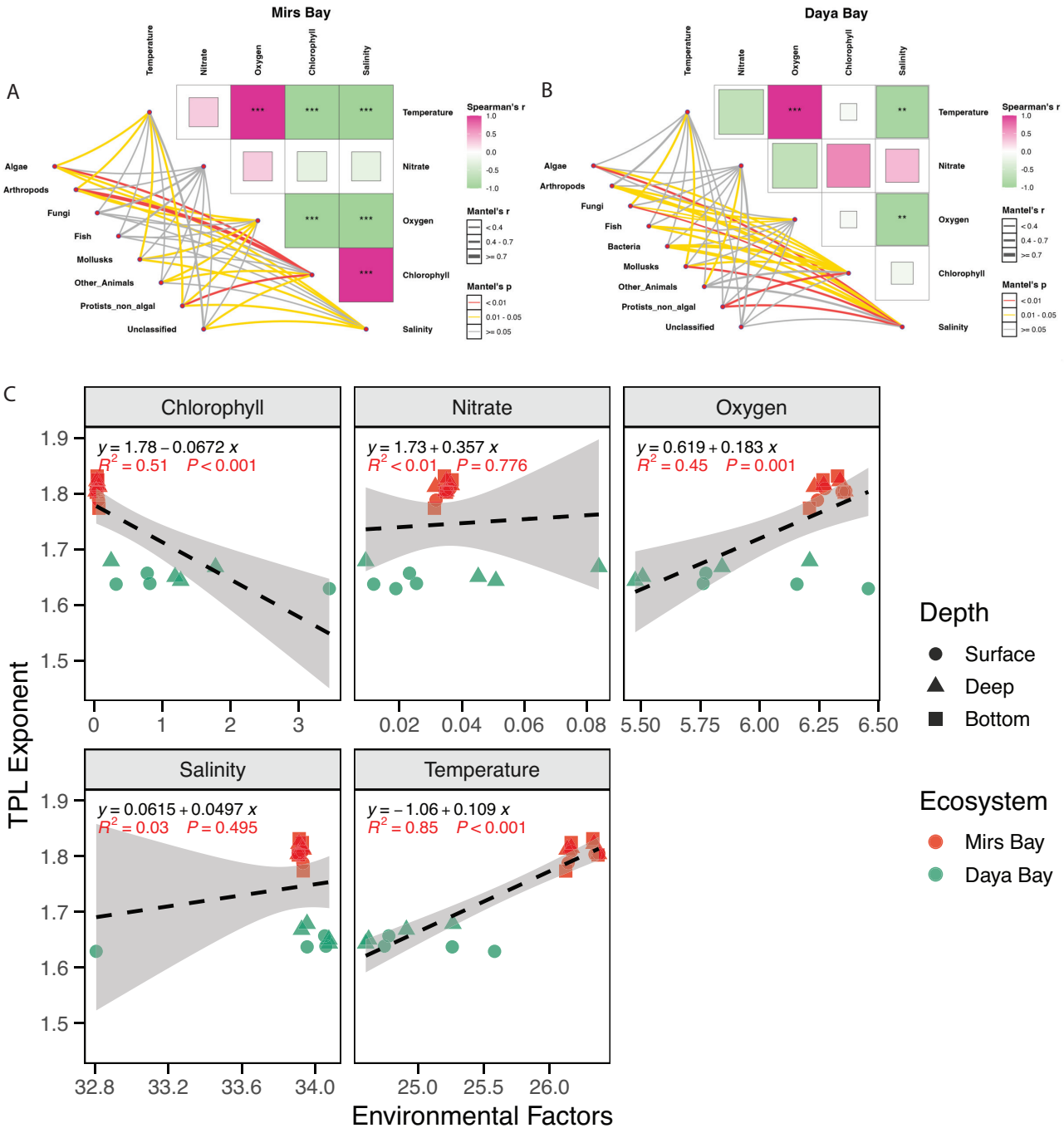

A
Mirs Bay
Temperature
Nitrate
Oxygen
Chlorophyll
Salinity
Algae
Arthropods
Fungi
Fish
Mollusks
Other_Animals
Protists_non_algal
Unclassified
Spearman's r
Mantel's r
Mantel's p
B
Daya Bay
Bacteria
C
Chlorophyll
y = 1.78 − 0.0672 x
R2 = 0.51 P < 0.001
Nitrate
y = 1.73 + 0.357 x
R2 < 0.01 P = 0.776
Oxygen
y = 0.619 + 0.183 x
R2 = 0.45 P = 0.001
Salinity
y = 0.0615 + 0.0497 x
R2 = 0.03 P = 0.495
Temperature
y = −1.06 + 0.109 x
R2 = 0.85 P < 0.001
TPL Exponent
Environmental Factors
Depth
Surface
Deep
Bottom
Ecosystem
Mirs Bay
Daya Bay

Figure 7:

Supplementary Information

S1 Supplementary Tables

Table S1. Environmental variables at sampling sites in Mirs Bay and Daya Bay. Hydrodynamical and biogeochemical parameters were retrieved from the WavyOcean database based on the geographic coordinates and sampling depths of each site. Values are year averages considering predicted daily data from 1992. The Mirs Bay includes four sampling habitats (Fig 2b): CN, DR, RR, and SR sampling points, and the Daya Bay includes HO1, HO2, IL, and XI sampling habitats (Fig 2c) (see Glossary for acronyms). Among these habitats, three communities where sampled: SW represents surface water, DW represents "deep" water (intermediate depth), and BO represents bottom water.

Table S2. Primers for eDNA metabarcoding amplification. List of primer pairs employed for environmental DNA (eDNA) amplification and subsequent sequencing. Each primer set is shown with its forward (F) and reverse (R) sequences in the 5'–3' orientation, expected amplicon length (bp), and the targeted genomic region. The MiFish-U/E primers target a highly conserved region of the mitochondrial 12S rRNA gene, widely used for fish metabarcoding. The DIV4 primer pair amplifies the eukaryotic nuclear 18S rRNA gene region, suitable for detecting a broad range of taxa. The Sauron-S878 and jgHCO2198 primers amplify a fragment of the mitochondrial cytochrome c oxidase subunit I gene (COI-5P), a standard barcode region for metazoans.

Table S3. Network topological metrics calculated for co-occurrence networks of microbial communities across sampling sites in Mirs Bay and Daya Bay. For each sample, the network was constructed based on molecular marker data, and key topological properties were quantified, including the number of nodes, average degree, average path length, betweenness centrality, network diameter, network density, and clustering coefficient. These metrics reflect differences in network complexity, connectivity, and modularity across sites and depths.

S2 Supplementary Figures

Figure S1. Preston's plot between Species Richness and Relative Species Abun-

dance for different taxonomic class. The Preston's plot is shown dependent on molecular barcode markers, and for all markers (ecosystem scale).

Figure S2. Preston's plot between Species Richness and Relative Species Abundance for different habitats. The Preston's plot is shown dependent on different habitats in Mirs and Daya bay for all markers.

Figure S3. Co-occurrence networks for communities in Mirs Bay. Each node represents an OTU, colored by its major taxonomic group (e.g., Algae, Fish, non-algal Protists). Edges indicate significant statistical correlations between OTUs.

Figure S4. Co-occurrence networks for communities in Daya Bay. Each node represents an OTU, colored by its major taxonomic group (e.g., Algae, Fish, non-algal Protists). Edges indicate significant statistical correlations between OTUs.

Figure S5. Taylor's Power Law of species variance-mean in Mirs Bay. The slope of the fitted regression line represents the TPL exponent ν, which quantifies the degree of aggregation. Each plot represents a taxon, color-coded by functional type—Algae, Arthropods, Fish, Fungi, Mollusks, Other Animals, Non-algal Protists, and Unclassified groups.

Figure S6. Taylor's Power Law of species variance-mean in Daya Bay. The slope of the fitted regression line represents the TPL exponent ν, which quantifies the degree of aggregation. Each plot represents a taxon, color-coded by functional type—Algae, Arthropods, Fish, Fungi, Mollusks, Other Animals, Non-algal Protists, and Unclassified groups.

Figure S7. Network-theoretic Kleiber's Law between RSA variance and node hyperconnectivity for taxa in Mirs Bay. Panels correspond to different taxonomic types (Algae, Arthropods, Fish, Fungi, Mollusks, Other Animals, Non-algal Protists, Unclassified), with regression lines indicating group-specific trends.

Figure S8. Network-theoretic Kleiber's Law between RSA variance and node hyperconnectivity for taxa in Daya Bay. Panels correspond to different taxonomic types

(Algae, Arthropods, Fish, Fungi, Mollusks, Other Animals, Non-algal Protists, Unclassified), with regression lines indicating group-specific trends.

Figure S9. Assumed linear relationships between environmental factors and cross-trophic network properties in Mirs Bay and Daya Bay. Plots display the assumed linear correlations between key topological parameters (nodes, degree, average path length, clustering coefficient, betweenness, network density, and network diameter) and environmental variables (chlorophyll-a, nitrate, dissolved oxygen, salinity, and temperature). Blue lines indicate regression fits, shaded areas represent 95% confidence intervals, and significance levels are reported for each test.

Figure S10. Relationships between Taylor's Power Law Exponent (TPL) and Network Topological features. This figure shows the linear relationships between the TPL exponent and seven key network topological parameters. Each point represents the network of a single sample. Colors indicate sampling regions (red: Mirs Bay; teal: Daya Bay), while shapes distinguish sampling depths. Dashed lines denote linear regression fits, with shaded gray areas representing the 95% confidence intervals.

Name	Location	Temperature (°C)	Nitrate (mmol/m^3)	Dissolved Oxygen (m/s)	Chlorophyll-a (mg/m^3)	Salinity (PSU)	Depth
SR-SW	Mirs Bay	26.1639	0.0363	6.2742	0.0560	33.9294	surface
SR-DW	Mirs Bay	26.1628	0.0366	6.2693	0.0565	33.9295	deep
SR-BO	Mirs Bay	26.1626	0.0369	6.2663	0.0562	33.9295	bottom
CN-SW	Mirs Bay	26.3724	0.0347	6.3626	0.0347	33.9070	surface
CN-DW	Mirs Bay	26.3693	0.0348	6.3588	0.0353	33.9073	deep
CN-BO	Mirs Bay	26.3661	0.0351	6.3551	0.0355	33.9077	bottom
DR-SW	Mirs Bay	26.3428	0.0355	6.3461	0.0438	33.9108	surface
DR-DW	Mirs Bay	26.3362	0.0350	6.3385	0.0456	33.9115	deep
DR-BO	Mirs Bay	26.3267	0.0344	6.3276	0.0476	33.9125	bottom
RR-SW	Mirs Bay	26.1396	0.0317	6.2433	0.0695	33.9327	surface
RR-DW	Mirs Bay	26.1326	0.0315	6.2303	0.0720	33.9334	deep
RR-BO	Mirs Bay	26.1213	0.0312	6.2096	0.0749	33.9346	bottom
HO1-SW	Daya Bay	24.7454	0.0255	5.7625	0.8201	34.0578	surface
HO1-DW	Daya Bay	24.6258	0.0453	5.5077	1.1897	34.0738	deep
HO2-SW	Daya Bay	24.7790	0.0232	5.7736	0.7818	34.0513	surface
HO2-DW	Daya Bay	24.6038	0.0509	5.4767	1.2707	34.0764	deep
XI-SW	Daya Bay	25.2604	0.0117	6.1568	0.3258	33.9555	surface
XI-DW	Daya Bay	25.2646	0.0092	6.2106	0.2527	33.9552	deep
IL-SW	Daya Bay	25.5813	0.0188	6.4571	3.4470	32.8072	surface
IL-DW	Daya Bay	24.9124	0.0840	5.8418	1.7811	33.9253	deep

Table S1:

Primer Pair	**Sequences (5′–3′)**	**Length (bp)**	**Region**
MiFish-U/E-F	5′–GTYGGTAAAWCTCGTGCCAGC–3′	∼183	12S
MiFish-U/E-R	5′–CATAGTGGGGTATCTAATCCYAGTTTG–3′	∼183	12S
DIV4_F	5′–GCGGTAATTCCAGCTCCAATAG–3′	∼315	18S
DIV4_R	5′–CTCTGACAATGGAATACGAATA–3′	∼315	18S
Sauron-S878	5′–GGDRCWGGWTGAACWGTWTAYCCNCC–3′	∼313	COI-5P
jgHCO2198	5′–TAIACYTCIGGRTGICCRAARAAYCA–3′	∼313	COI-5P

Table S2:

Name	Network Size	Average Degree	Average Shortest Path Length	Average Betweenness Centrality	Average Clustering Coefficient	Network Density	Network Diameter
SR-SW	679	2.698	7.890	0.052	0.362	0.00398	26.656
SR-DW	688	2.654	8.041	0.059	0.359	0.00386	26.708
SR-BO	675	2.631	8.554	0.088	0.361	0.00390	30.380
CN-SW	725	2.745	7.189	0.044	0.431	0.00379	20.394
CN-DW	692	2.725	7.299	0.047	0.436	0.00394	21.300
CN-BO	677	2.792	7.344	0.051	0.430	0.00413	21.300
DR-SW	667	2.564	8.806	0.067	0.373	0.00385	26.677
DR-DW	623	2.629	7.520	0.080	0.366	0.00423	25.856
DR-BO	623	2.626	7.913	0.080	0.368	0.00422	24.915
RR-SW	608	2.503	6.983	0.057	0.365	0.00412	21.144
RR-DW	678	2.584	8.823	0.074	0.363	0.00382	30.380
RR-BO	663	2.658	8.394	0.066	0.362	0.00401	26.708
HO1-SW	4635	2.861	8.495	0.004	0.712	0.00062	28.570
HO1-DW	4315	2.693	8.378	0.004	0.700	0.00062	29.527
HO2-SW	4220	2.742	8.411	0.005	0.711	0.00065	28.570
HO2-DW	4416	2.770	8.963	0.005	0.718	0.00063	30.521
IL-SW	4099	2.546	4.211	0.000	0.796	0.00062	19.710
IL-DW	3711	2.357	8.713	0.003	0.802	0.00064	25.644
XI-SW	4704	3.146	8.355	0.004	0.744	0.00067	28.570
XI-DW	3540	2.493	8.477	0.005	0.710	0.00070	28.570

Table S3:

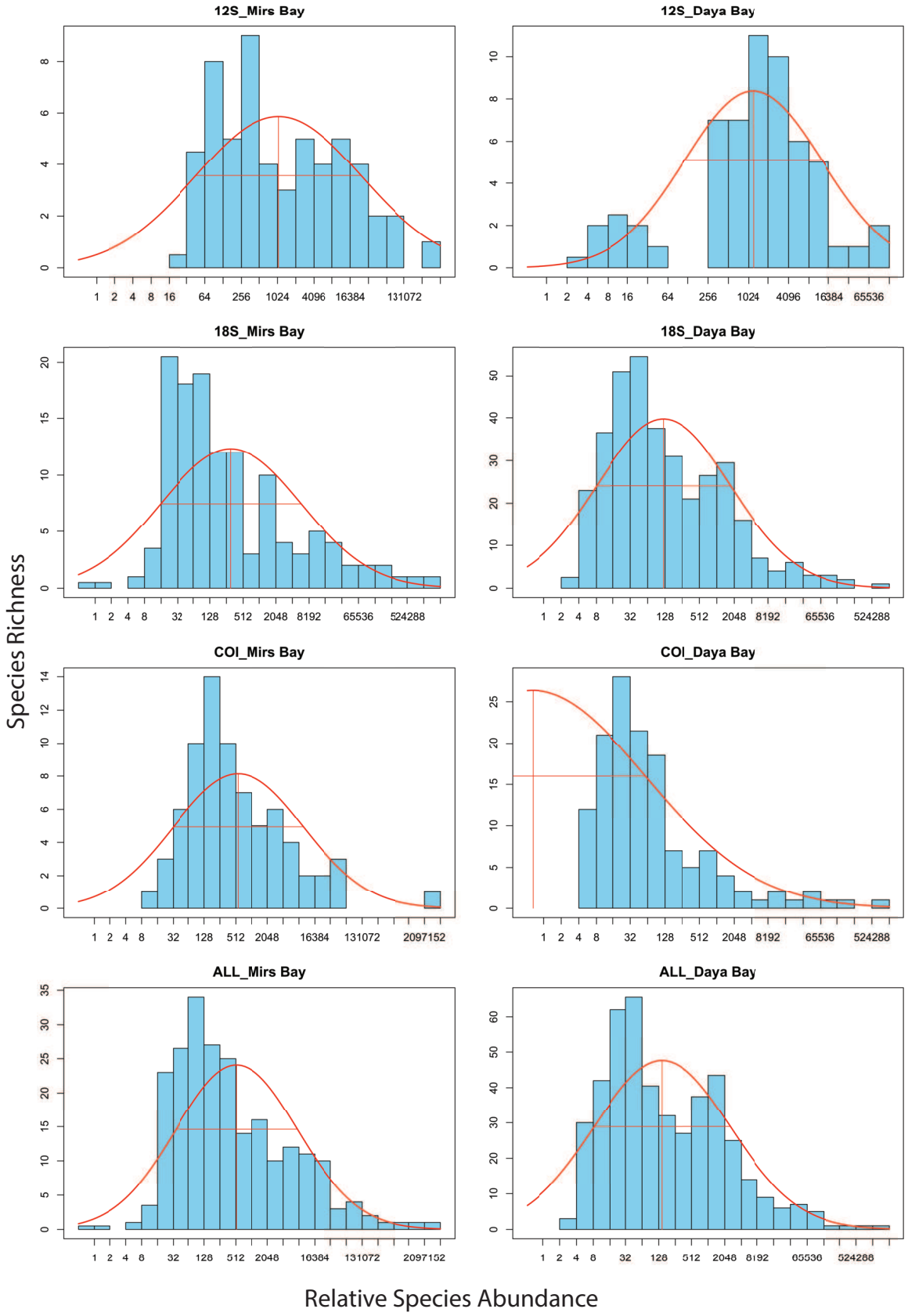

12S_Mirs Bay
12S_Daya Bay
18S_Mirs Bay
18S_Daya Bay
COI_Mirs Bay
COI_Daya Bay
ALL_Mirs Bay
ALL_Daya Bay
Species Richness
Relative Species Abundance

Figure S1:

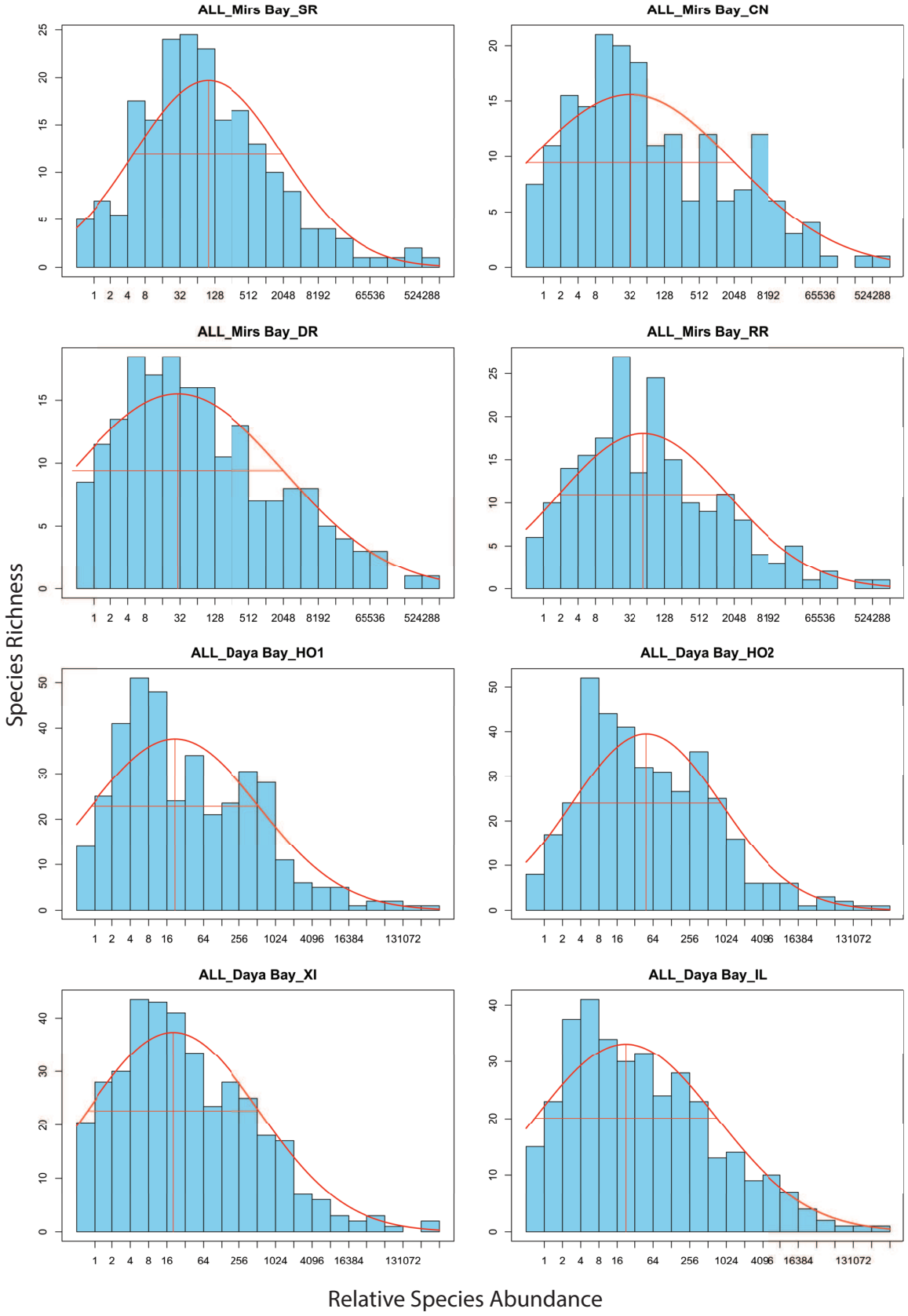

ALL_Mirs Bay_SR
ALL_Mirs Bay_CN
ALL_Mirs Bay_DR
ALL_Mirs Bay_RR
ALL_Daya Bay_HO1
ALL_Daya Bay_HO2
ALL_Daya Bay_XI
ALL_Daya Bay_IL
Species Richness
Relative Species Abundance

Figure S2:

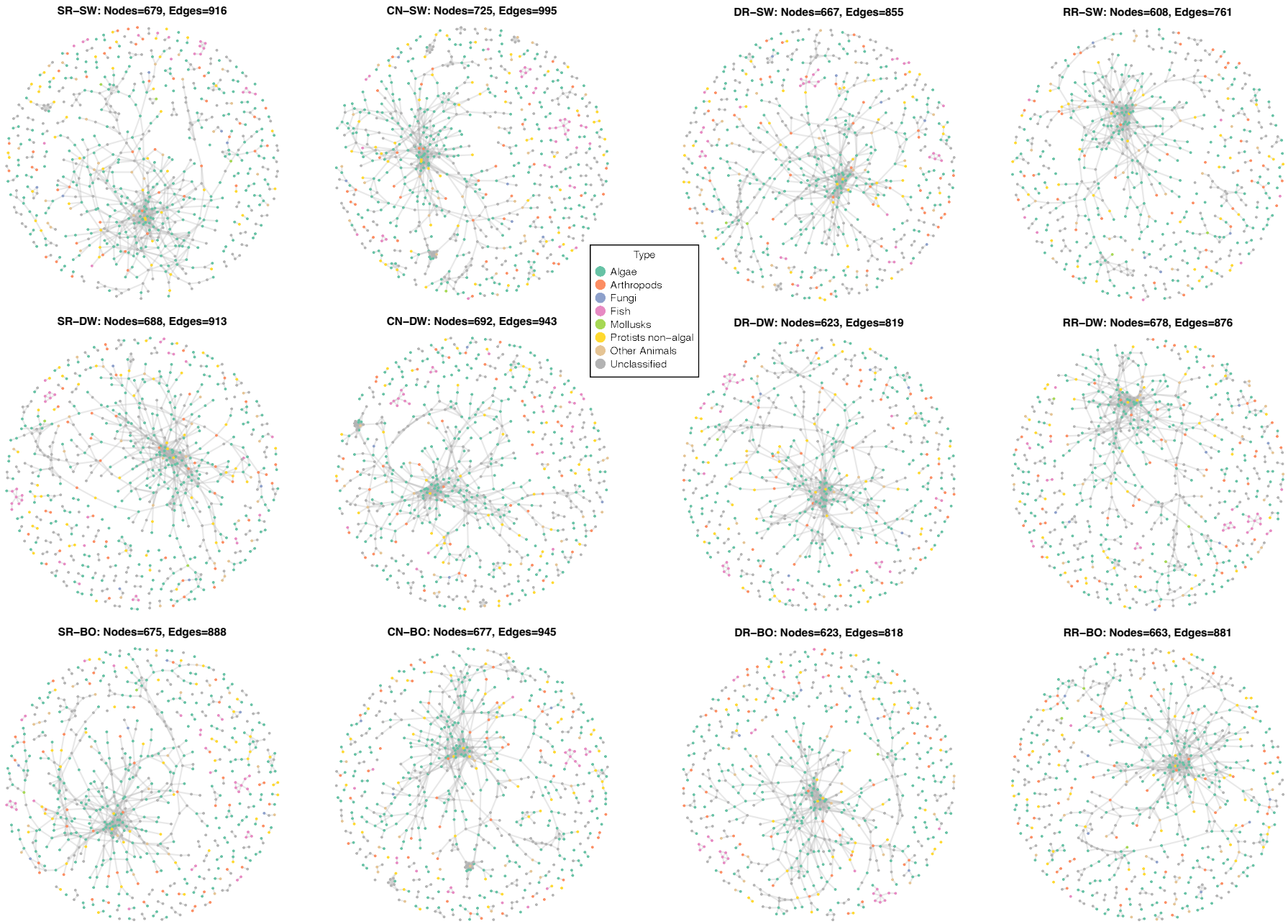

SR–SW: Nodes=679, Edges=916
CN–SW: Nodes=725, Edges=995
DR–SW: Nodes=667, Edges=855
RR–SW: Nodes=608, Edges=761
SR–DW: Nodes=688, Edges=913
CN–DW: Nodes=692, Edges=943
DR–DW: Nodes=623, Edges=819
RR–DW: Nodes=678, Edges=876
SR–BO: Nodes=675, Edges=888
CN–BO: Nodes=677, Edges=945
DR–BO: Nodes=623, Edges=818
RR–BO: Nodes=663, Edges=881
Type
Algae
Arthropods
Fungi
Fish
Mollusks
Protists non–algal
Other Animals
Unclassified

Figure S3:

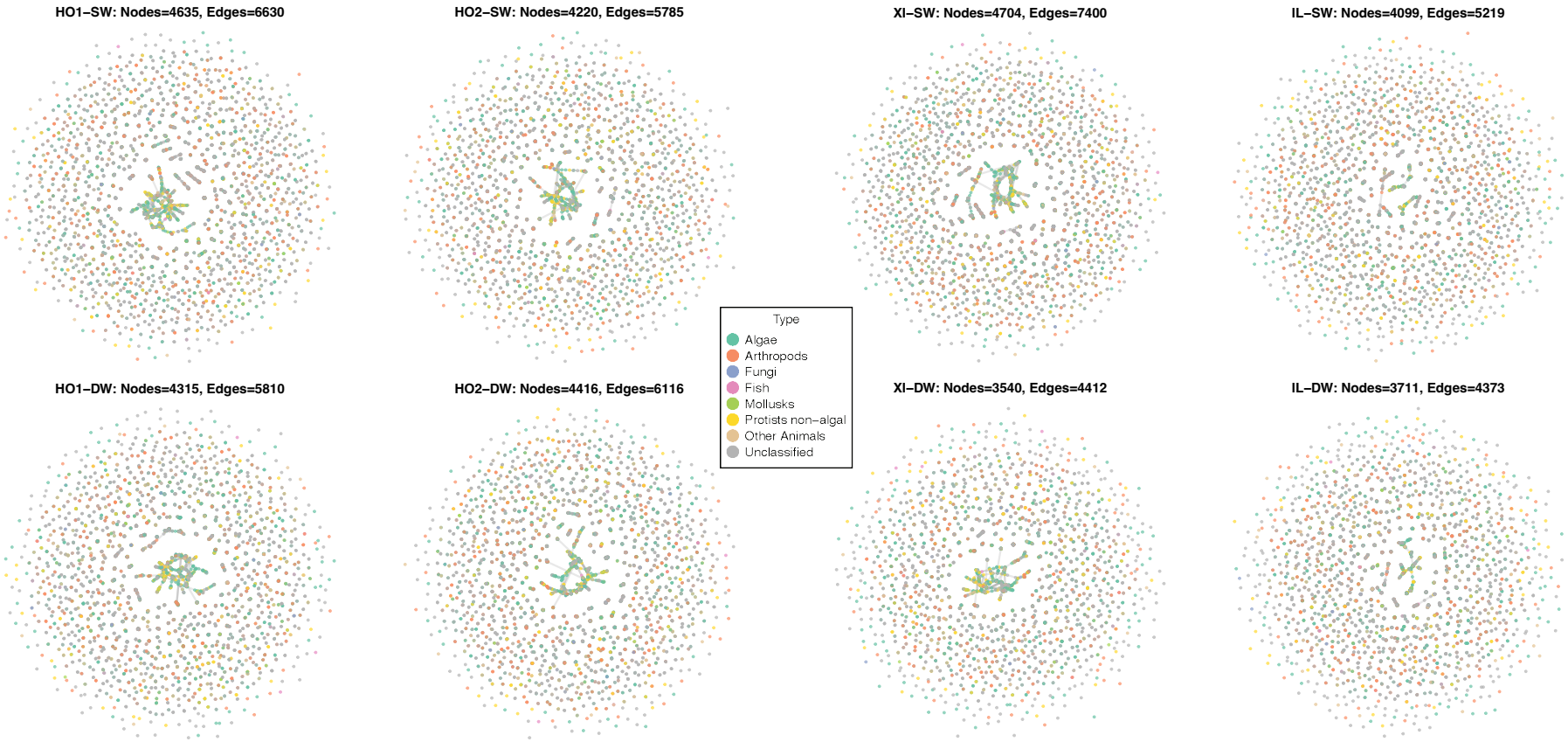

HO1−SW: Nodes=4635, Edges=6630
HO2−SW: Nodes=4220, Edges=5785
XI−SW: Nodes=4704, Edges=7400
IL−SW: Nodes=4099, Edges=5219
HO1−DW: Nodes=4315, Edges=5810
HO2−DW: Nodes=4416, Edges=6116
XI−DW: Nodes=3540, Edges=4412
IL−DW: Nodes=3711, Edges=4373
Type
Algae
Arthropods
Fungi
Fish
Mollusks
Protists non−algal
Other Animals
Unclassified

Figure S4:

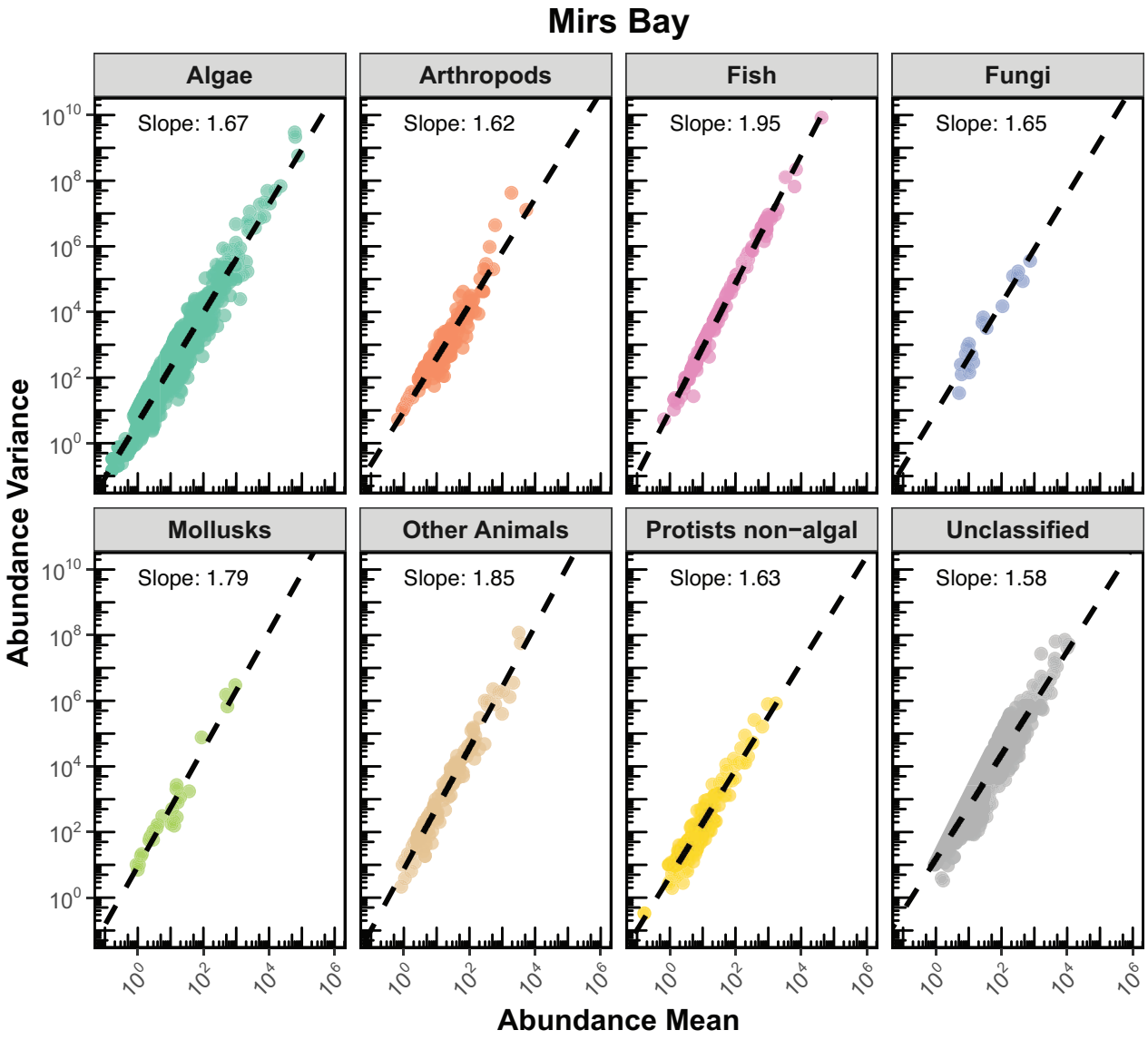

Mirs Bay
Algae
Arthropods
Fish
Fungi
Mollusks
Other Animals
Protists non−algal
Unclassified
Slope: 1.67
Slope: 1.62
Slope: 1.95
Slope: 1.65
Slope: 1.79
Slope: 1.85
Slope: 1.63
Slope: 1.58
Abundance Variance
Abundance Mean

Figure S5:

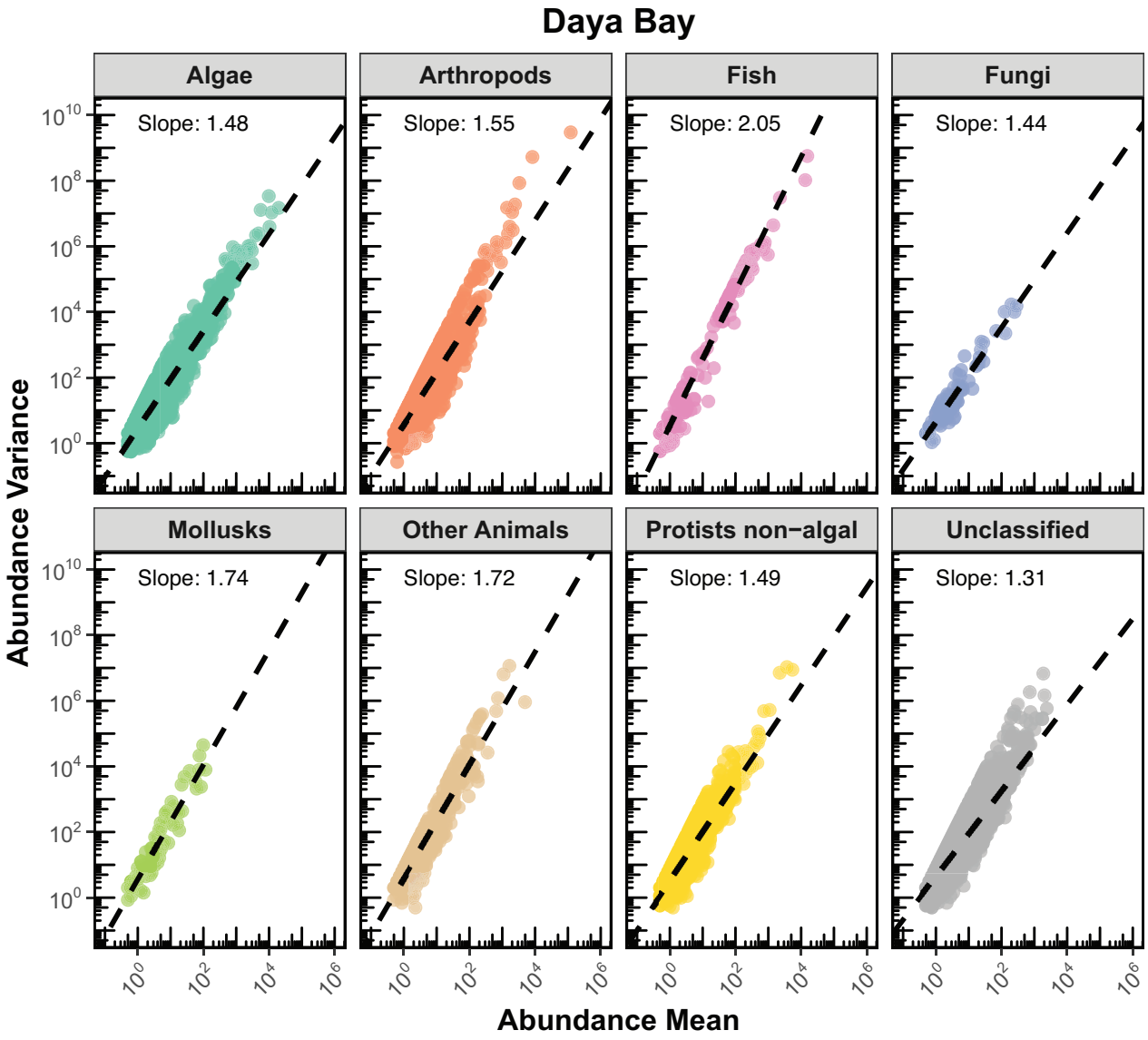

Daya Bay
Algae
Slope: 1.48
Arthropods
Slope: 1.55
Fish
Slope: 2.05
Fungi
Slope: 1.44
Mollusks
Slope: 1.74
Other Animals
Slope: 1.72
Protists non−algal
Slope: 1.49
Unclassified
Slope: 1.31
Abundance Variance
Abundance Mean

Figure S6:

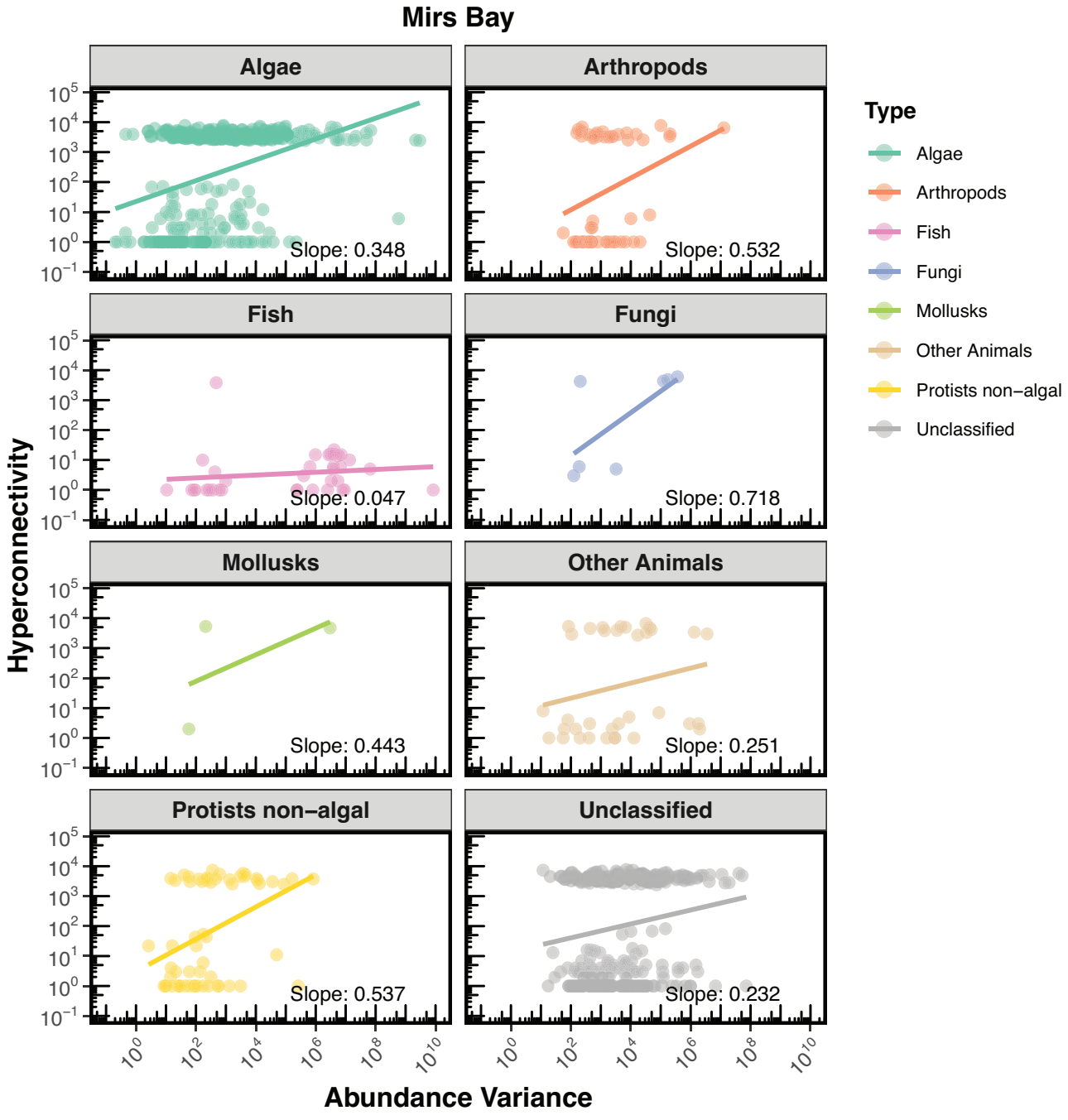

Mirs Bay
Algae
Arthropods
Fish
Fungi
Mollusks
Other Animals
Protists non−algal
Unclassified
Slope: 0.348
Slope: 0.532
Slope: 0.047
Slope: 0.718
Slope: 0.443
Slope: 0.251
Slope: 0.537
Slope: 0.232
Hyperconnectivity
Abundance Variance
Type
Algae
Arthropods
Fish
Fungi
Mollusks
Other Animals
Protists non−algal
Unclassified

Figure S7:

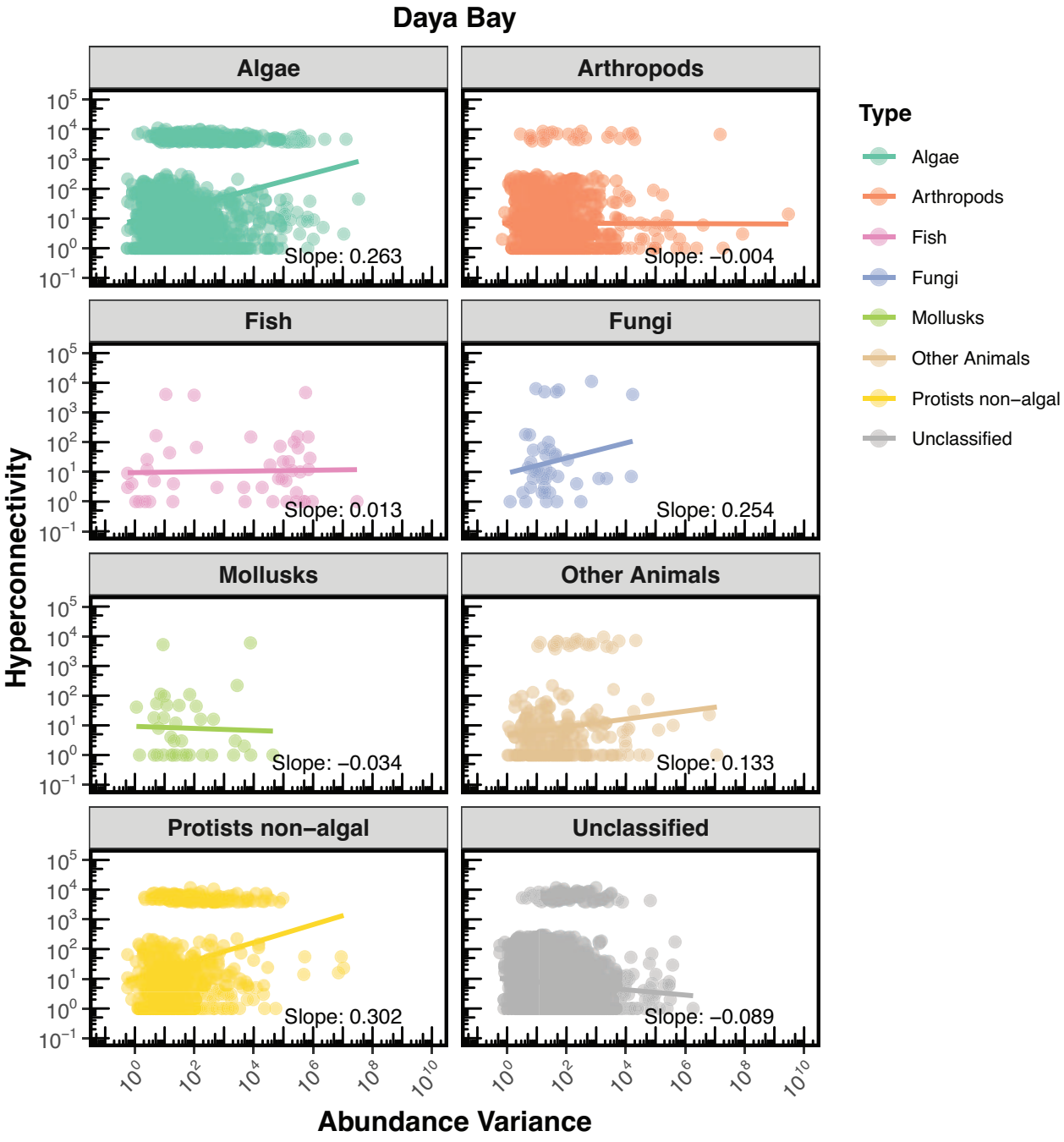

Daya Bay
Algae
Arthropods
Fish
Fungi
Mollusks
Other Animals
Protists non–algal
Unclassified
Slope: 0.263
Slope: –0.004
Slope: 0.013
Slope: 0.254
Slope: –0.034
Slope: 0.133
Slope: 0.302
Slope: –0.089
Hyperconnectivity
Abundance Variance
Type
Algae
Arthropods
Fish
Fungi
Mollusks
Other Animals
Protists non–algal
Unclassified

Figure S8:

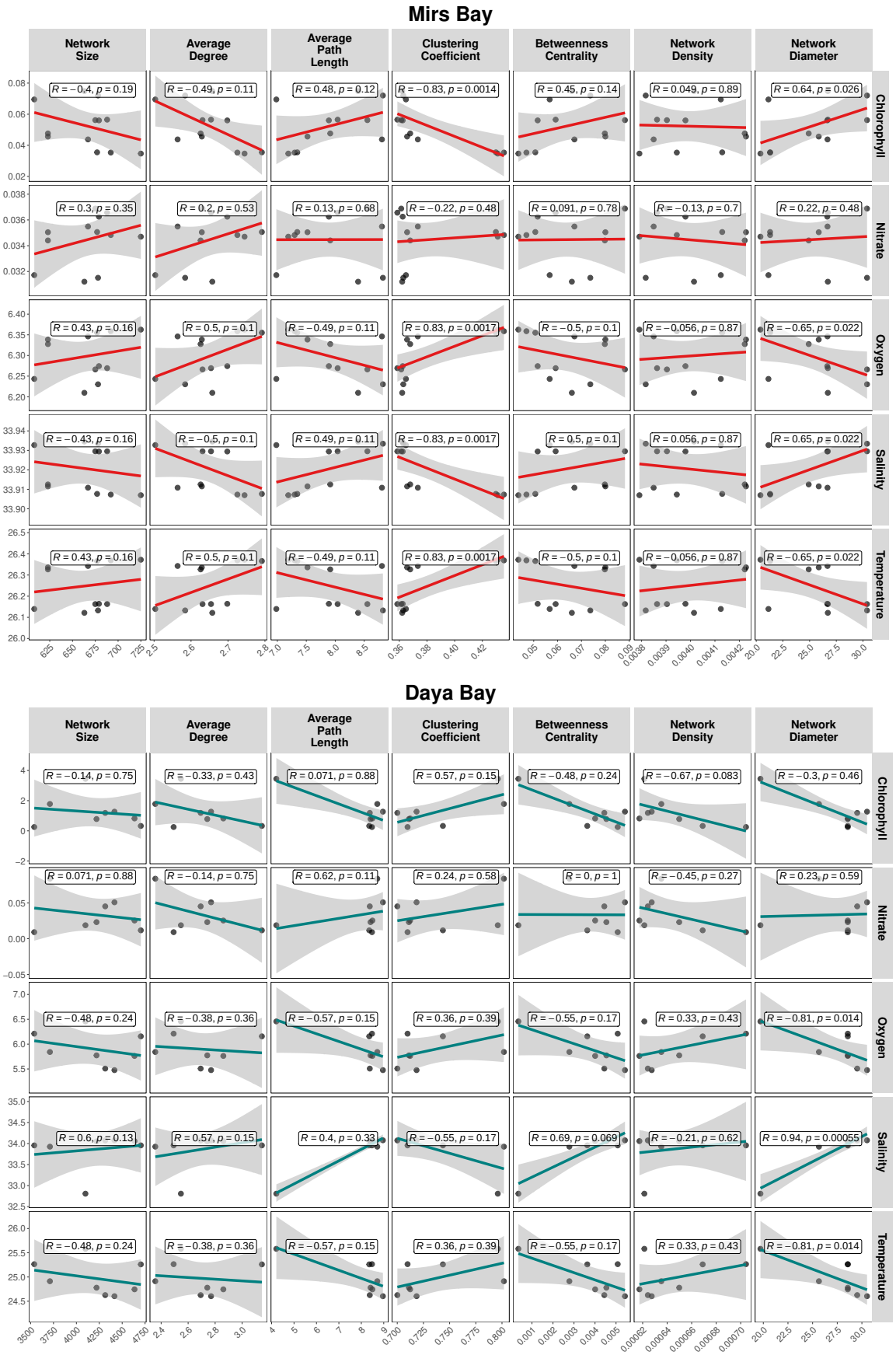

Mirs Bay
Network Size
Average Degree
Average Path Length
Clustering Coefficient
Betweenness Centrality
Network Density
Network Diameter
Chlorophyll
Nitrate
Oxygen
Salinity
Temperature
R = −0.4, p = 0.19
R = −0.49, p = 0.11
R = 0.48, p = 0.12
R = −0.83, p = 0.0014
R = 0.45, p = 0.14
R = 0.049, p = 0.89
R = 0.64, p = 0.026
R = 0.3, p = 0.35
R = 0.2, p = 0.53
R = 0.13, p = 0.68
R = −0.22, p = 0.48
R = 0.091, p = 0.78
R = −0.13, p = 0.7
R = 0.22, p = 0.48
R = 0.43, p = 0.16
R = 0.5, p = 0.1
R = −0.49, p = 0.11
R = 0.83, p = 0.0017
R = −0.5, p = 0.1
R = −0.056, p = 0.87
R = −0.65, p = 0.022
R = −0.43, p = 0.16
R = −0.5, p = 0.1
R = 0.49, p = 0.11
R = −0.83, p = 0.0017
R = 0.5, p = 0.1
R = 0.056, p = 0.87
R = 0.65, p = 0.022
R = 0.43, p = 0.16
R = 0.5, p = 0.1
R = −0.49, p = 0.11
R = 0.83, p = 0.0017
R = −0.5, p = 0.1
R = −0.056, p = 0.87
R = −0.65, p = 0.022
Daya Bay
Network Size
Average Degree
Average Path Length
Clustering Coefficient
Betweenness Centrality
Network Density
Network Diameter
Chlorophyll
Nitrate
Oxygen
Salinity
Temperature
R = −0.14, p = 0.75
R = −0.33, p = 0.43
R = 0.071, p = 0.88
R = 0.57, p = 0.15
R = −0.48, p = 0.24
R = −0.67, p = 0.083
R = −0.3, p = 0.46
R = 0.071, p = 0.88
R = −0.14, p = 0.75
R = 0.62, p = 0.11
R = 0.24, p = 0.58
R = 0, p = 1
R = −0.45, p = 0.27
R = 0.23, p = 0.59
R = −0.48, p = 0.24
R = −0.38, p = 0.36
R = −0.57, p = 0.15
R = 0.36, p = 0.39
R = −0.55, p = 0.17
R = 0.33, p = 0.43
R = −0.81, p = 0.014
R = 0.6, p = 0.13
R = 0.57, p = 0.15
R = 0.4, p = 0.33
R = −0.55, p = 0.17
R = 0.69, p = 0.069
R = −0.21, p = 0.62
R = 0.94, p = 0.00055
R = −0.48, p = 0.24
R = −0.38, p = 0.36
R = −0.57, p = 0.15
R = 0.36, p = 0.39
R = −0.55, p = 0.17
R = 0.33, p = 0.43
R = −0.81, p = 0.014

Figure S9:

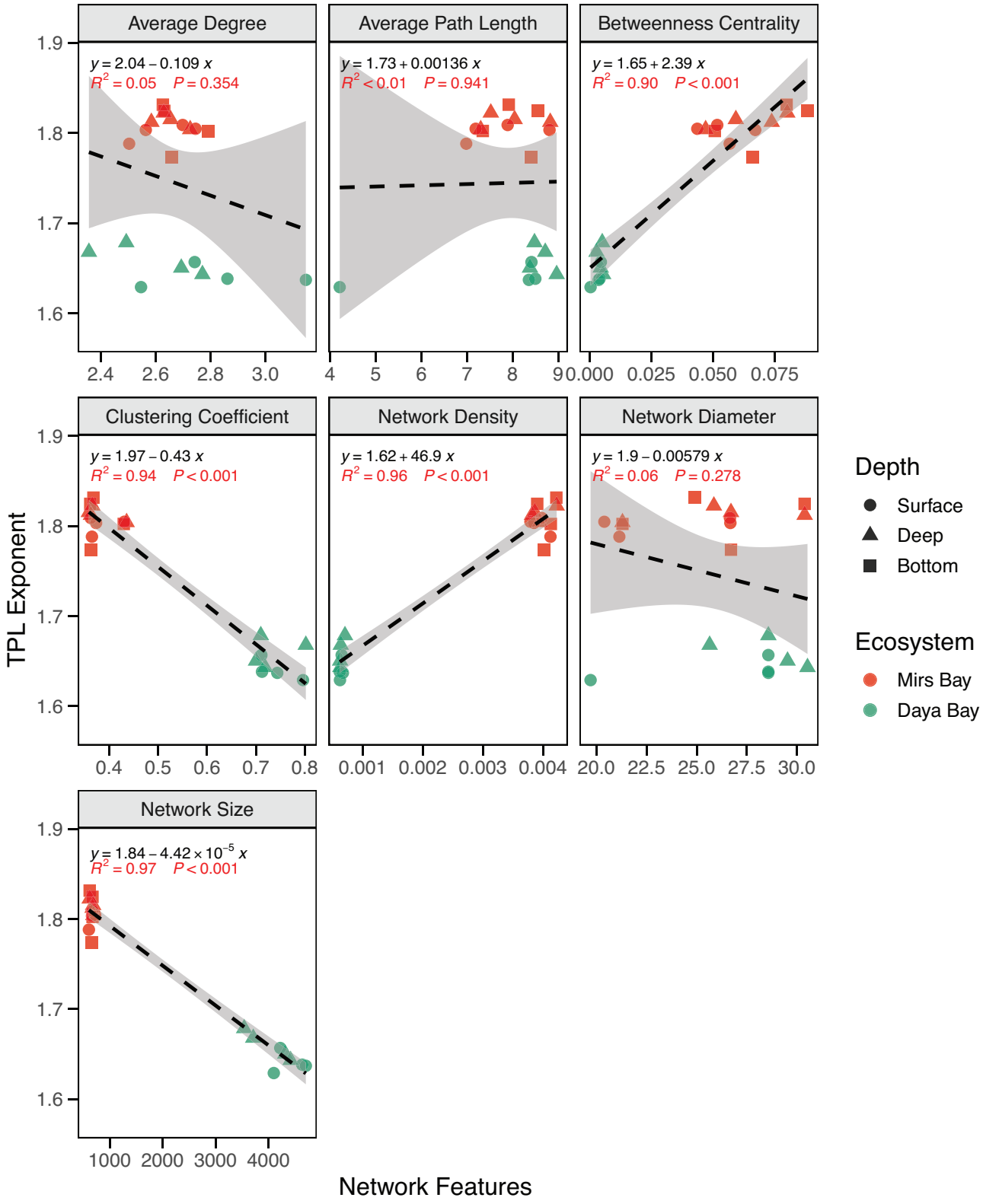

Average Degree
y = 2.04 − 0.109 x
R² = 0.05 P = 0.354
Average Path Length
y = 1.73 + 0.00136 x
R² < 0.01 P = 0.941
Betweenness Centrality
y = 1.65 + 2.39 x
R² = 0.90 P < 0.001
Clustering Coefficient
y = 1.97 − 0.43 x
R² = 0.94 P < 0.001
Network Density
y = 1.62 + 46.9 x
R² = 0.96 P < 0.001
Network Diameter
y = 1.9 − 0.00579 x
R² = 0.06 P = 0.278
Network Size
y = 1.84 − 4.42 × 10⁻⁵ x
R² = 0.97 P < 0.001
TPL Exponent
Network Features
Depth
Surface
Deep
Bottom
Ecosystem
Mirs Bay
Daya Bay

Figure S10: